Experimental Validation of the Molecular Weight Distribution (MWD) and Chemical Composition Distribution (CCD) Deconvolution Method for Polyolefins Made with Ziegler-Natta Catalysts

by

Raunil Raj

A thesis submitted in partial fulfillment of the requirements for the degree of

Master of Science

in

Chemical Engineering

Department of Chemical and Materials Engineering
University of Alberta

Abstract

Polyolefins are important commodity polymers. They account for more than 50 wt% of the total polymers produced in the world. Ziegler-Natta and Phillips catalysts, discovered in 1950, revolutionized the material science arena. Even 70 years after their invention, they continue to be responsible for most of the polyolefin production.

Ethylene/1-olefin copolymers made with Ziegler-Natta or Phillips catalysts have broad molecular weight distributions (MWD), a deviation from Flory most probable distribution. Additionally, their average 1-olefin content depends on polymer molecular weight, a deviation from Stockmayer distribution. This behavior is attributed to the presence of more than one type of active site in these catalysts. Numerical deconvolution methods have been used to estimate the minimum number of active site types needed to explain the microstructure of polyolefins made with these catalysts. These methods have been used to successfully describe polyolefins made in laboratory and industrial reactors, permit the development of useful simulation programs, but have never been tested from a fundamental point of view.

In this thesis, I developed a method to validate these deconvolution techniques experimentally. I synthesized ethylene/1-hexene copolymers with a commercial Zeigler-Natta catalyst, and measured and deconvoluted their molecular weight distribution (MWD) and chemical composition distribution (CCD) to determine the minimum number of Flory/Stockmayer polymer populations needed to represent these distributions. Then, I synthesized polymers with these single-site distributions with a metallocene catalyst and blended them in the proportions determined by the deconvolution procedure to find out whether these blends had the same microstructural properties of the polymers made with the multi-site Zeigler-Natta catalyst. In the

process, I established different deconvolution approaches to enhance the predictive power of this proposed method.

Dedication

To my father, Late Dr. Raj Kumar Upadhaya, who sacrificed and endured silently so I could succeed.

Acknowledgments

I wish to express my gratitude to a lot of people who have supported me during my MSc program at the University of Alberta.

I am grateful to my thesis supervisor Professor João B.P. Soares for not only his guidance, support, and supervision throughout the work but also for his care and affection in my life. I have learned so much about polyolefins, photography, and kindness from him.

I would like to thank my colleagues Venugopal Hegde, Amirreza Badri, Bao Liu, and Benjamin Nguyen for supporting and teaching me so much. And, to Linda Kaert especially for the much-needed emotional support and time. Special thanks to Dr. Saeid Mehdiabadi for his coaching and encouragement throughout my project.

I would like to thank my manager, Chad Gendall, for supporting and sharing my responsibilities so I could focus on my thesis.

My deepest gratitude to my mother for her sacrifices, resolute and love that inspired me to keep going. I have immense gratitude to my brother, Rohit Kumar, who not only coached me into getting an admit at this prestigious institution but always stood behind me in the arduous grad life that followed. I am truly grateful to my uncle, aunt, and the entire family for taking care of me in every way possible through the several ups and downs of life, not just during the MSc program. Finally, I wish to thank my fiancée Adriana Rivolta for actively and successfully finding ways to support me through this journey.

Table of Contents

List of Figures

List of Tables

Chapter 1
Introduction

Our modern world is unimaginable without polymers. Figure 1.1 describes various major applications where polymers are used today, which include packaging, building and construction, automotive, electrical and electronics, and others.[1] Polymers have been able to replace conventional materials like paper, wood, metal, and ceramics in a variety of applications owing to their low production cost, high chemical resistance, light weight, and superior mechanical properties.

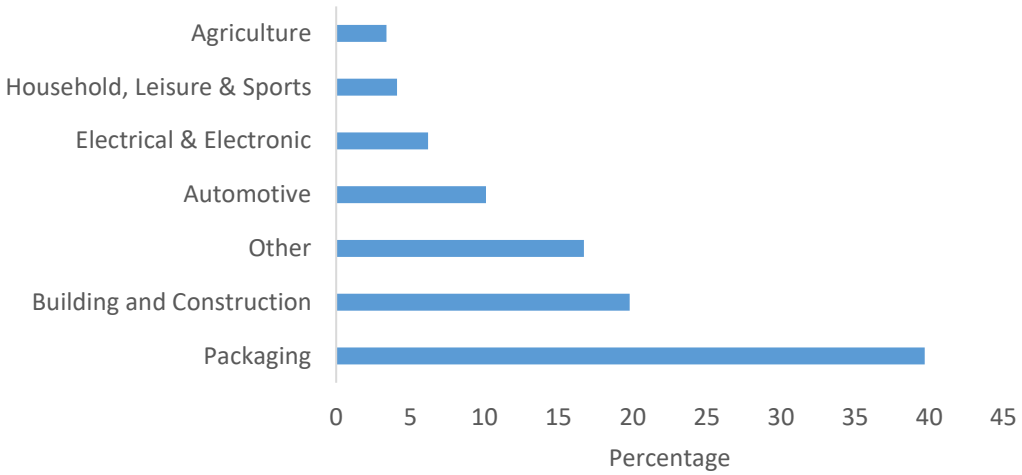

Figure 1-1 Applications of polymers in various industries in 2018.[1]

Polyolefins are a class of polymers formed by polymerizing olefins such as ethylene, propylene, 1-butene, and higher 1-olefins. Polyethylene is an important subclass among polyolefins. Figure 1.2 shows that polyethylene (high density polyethylene, HDPE; low density polyethylene, LDPE; and linear low density polyethylene, LLDPE) alone comprised about 28.5% of the total production of polymers worldwide in 2018.[2]

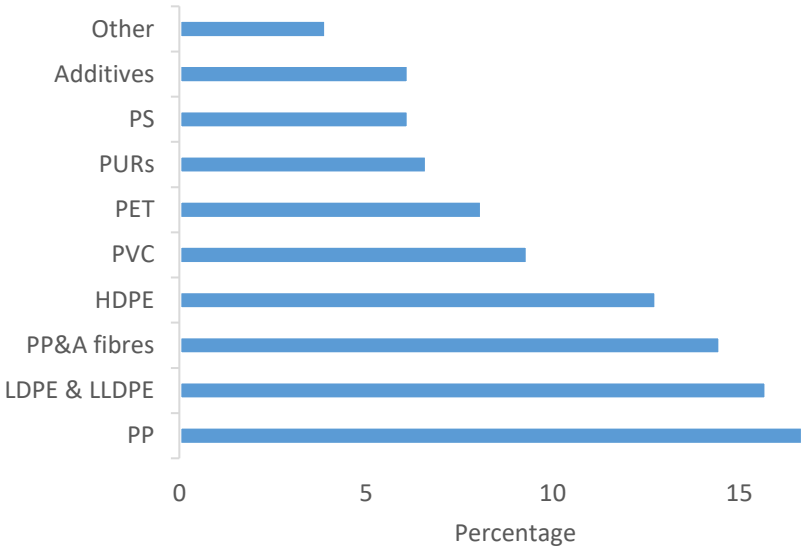

Figure 1-2 Proportions of different polymer production worldwide in 2018.[2]

Polyethylene resins, unlike their name, may make you infer, can be homopolymers of ethylene or copolymers of ethylene and 1-olefins. They are homopolymers when made using free-radical initiators, and mostly copolymers when made using coordination catalysts. Most commercial polyethylene resins are copolymers of ethylene and 1-butene, 1-hexene, or 1-octene.

The traditional classification of polyethylene is based upon their density range. They are broadly classified into three categories: low-density polyethylene (LDPE, 0.915-0.940 g cm^{-3}), linear low-density polyethylene (LLDPE, 0.915-0.94 g cm^{-3}), and high-density polyethylene (HDPE, 0.945-0.97 g cm^{-3}), as illustrated in Figure 1-3.[3]

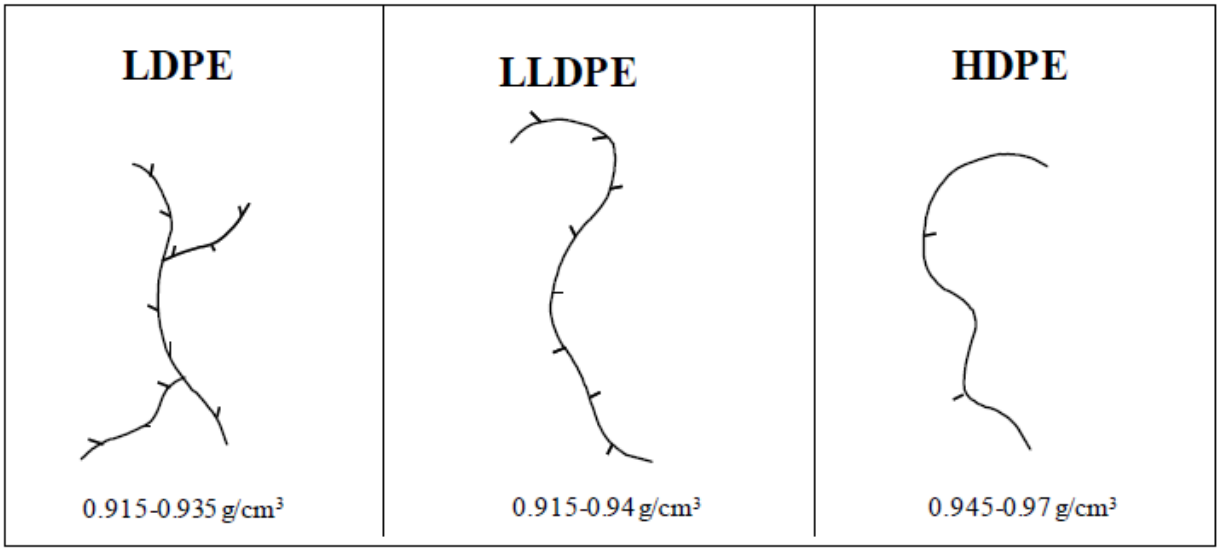

Figure 1-3 Polyethylene classification based on branching: LDPE, LLDPE, and HDPE.[3]

Density is an important property of polyethylene as it dictates its final application. Although the density is slightly influenced by molecular weight, it is largely affected by different branching structures in the polymer chains: short-chain branching (SCB) and long-chain branching (LCB).[4] These branches act as defects that prevent the chains from forming dense crystals. As a result, the SCB frequency increases, the density, crystallinity, and melting point of the polymer decreases. Therefore, LDPE with the highest frequency of SCB generally has a lower density in comparison to LLDPE and HDPE which due to their decreasing SCB frequencies, have higher densities. Regarding the final properties, LDPE is a tougher material, while LLDPE and HDPE have higher tensile strength.

Consequently, controlling the frequencies of SCB and LCB in the chains is instrumental in tailoring the final properties of polyethylene for different applications. LLDPE and HDPE are made by coordination polymerization. SCB in LLDPE and HDPE are formed by copolymerizing α-olefin comonomers (typically 1-butene, 1-hexene, and 1-octene) with ethylene, as shown in Figure 1-4.[3] The length of the SCB depends on the size of the α-olefin comonomer used. The formation of LCB in coordination polymerization, although not common, happens through a

copolymerization reaction with a polymer chain having a terminal vinyl group (macromonomer).[5]

Density (an average measure of branching structure and crystallinity in polyolefins) has been useful in getting a basic idea of the material properties in the past. However, the microstructure of commercial polyethylene is too complex to be captured with a single density value.[3] Thus, detailed knowledge of the microstructure of polyethylene, as given by its molecular weight distribution (MWD) and chemical composition distribution (CCD) (or short-chain branching distribution, SCBD) is needed to define the performance of products made with polyethylene. [6]

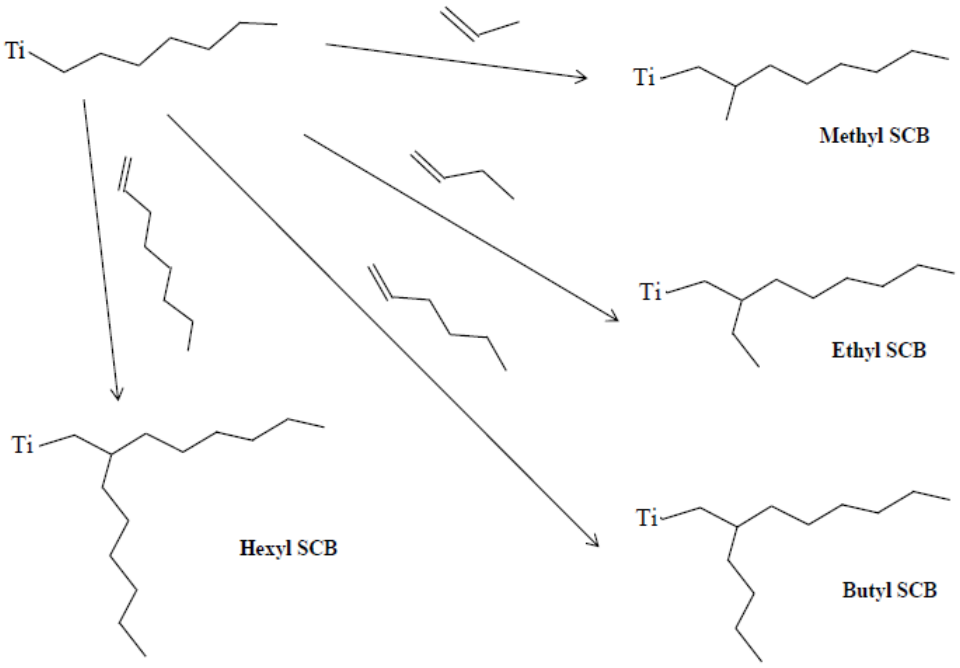

Figure 1-4 SCB formation mechanism in the coordination polymerization of ethylene and α-olefins.[3]

1.1 Motivation and Objectives

Most of the commercial polyethylene is produced with Ziegler Natta catalysts.[7] Their MWD and CCD are broad and non-uniform and do not follow Flory most probable distribution and Stockmayer distribution, respectively. This behavior is attributed to the presence of more than one type of active site in these catalysts.[8–11] Numerical deconvolution methods have been used to estimate the minimum number of active site types needed to explain the microstructure of polyolefins made with these catalysts.[12–15] These methods have been used to successfully describe polyolefins made in the laboratory and industrial reactors, but they have never been tested from a fundamental point of view. Validating these methods experimentally was the focus of this thesis. Additionally, new deconvolution methods were developed to further increase their predictive power.

1.2 Thesis Outline

A brief overview of the background of polyethylene microstructure, their methods of characterization, and the nature of the catalysts used to make polyethylene are given in Chapter 2. Experimental procedures and materials used to make copolymers using Zeigler-Natta catalyst (multi-site) and metallocene catalysts (single-site) are described in Chapter 3. Different deconvolution approaches are compared in Chapter 4. Conclusion and recommendations for future work are given in Chapter 5.

Chapter 2
Literature Review

2.1 Polyethylene Microstructural Distributions and Characterization

Polyethylene microstructural distributions, such as molecular weight distribution, chemical composition distribution (or short-chain branching distribution) are characterized by gel permeation chromatography (GPC), differential scanning calorimetry (DSC), and crystallization based techniques like crystallization analysis fractionation (CRYSTAF), temperature rising elution fractionation (TREF), and crystallization elution fractionation (CEF). Brief introductions of these analytical techniques are given in the following sections.

2.1.1 Molecular Weight Distribution

Molecular weight distribution (MWD) is the most fundamental property of a polymer. Polyethylene is no exception to the rule.[16] Depending upon the application, the molecular weight of polyethylene can range from several hundred (low molecular weight resins used as hot melt adhesives) to a few million (ultra-high molecular weight polyethylene, UHMWPE, a high-performance fiber).[17] However, unlike small molecules, which have a defined molecular weight, due to the stochastic nature of polymerization reactions, polymers are mixtures of molecules of different molecular weights. Different averages, such as the number average molecular weight (M_n) and the weight average molecular weight (M_w) are used to quantify the averages and breadth of the molecular weight distribution of a given polymer. The averages are defined as,

$$M_n = \frac{\sum N_i M_i}{\sum N_i} \tag{2.1}$$

$$M_w = \frac{\sum N_i M_i^2}{\sum N_i M_i} = \sum w_i M_i \tag{2.2}$$

where, M_i is the molecular weight of the polymer chains, N_i is the number of the polymer chains whose molecular weight is M_i, and w_i is the weight fraction of the chains whose molecular weight is M_i.

The breadth of the underlying molecular weight distribution is quantified with the ratio M_w/M_n. In polyolefins, this ratio is still mostly called the polydispersity index (PDI), even though IUPAC now recommends the term dispersity (D). For many applications, however, using one or more molecular weight averages is not enough to describe the polymer properties and the whole molecular weight distribution must be reported. Fortunately, with the advent of advanced characterization equipment such as gel permeation chromatography (GPC), measuring the MWD is fast and relatively easy.

Gel permeation chromatography has been routinely used to measure the MWD of polyethylene, as schematically illustrated in Figure 2-1.[18] In this method, a solution of the polyethylene sample (analyte) is prepared in a solvent (typically trichlorobenzene, TCB, or o-dichlorobenzene, ODCB). The solution is then pumped through a series of columns filled with porous packing material. Larger molecules pass through the column without spending much time in the pores and have shorter elution times. As the progressively smaller molecules pass through the packing material, they enter increasingly smaller pores and spend more time in the column. In this way, molecules, are separated based on the volume they occupy in the solution (hydrodynamic volume). [5,19] The hydrodynamic volume of a polymer chain depends on its chain length, branching topology, solvent type, temperature, and polymer solution concentration. To eliminate the effect of polymer solution concentration, the polymer solutions are kept as dilute as possible. The volume of linear polyethylene chains with the same SCB frequency is directly proportional to their chain lengths or molecular weights.[3]

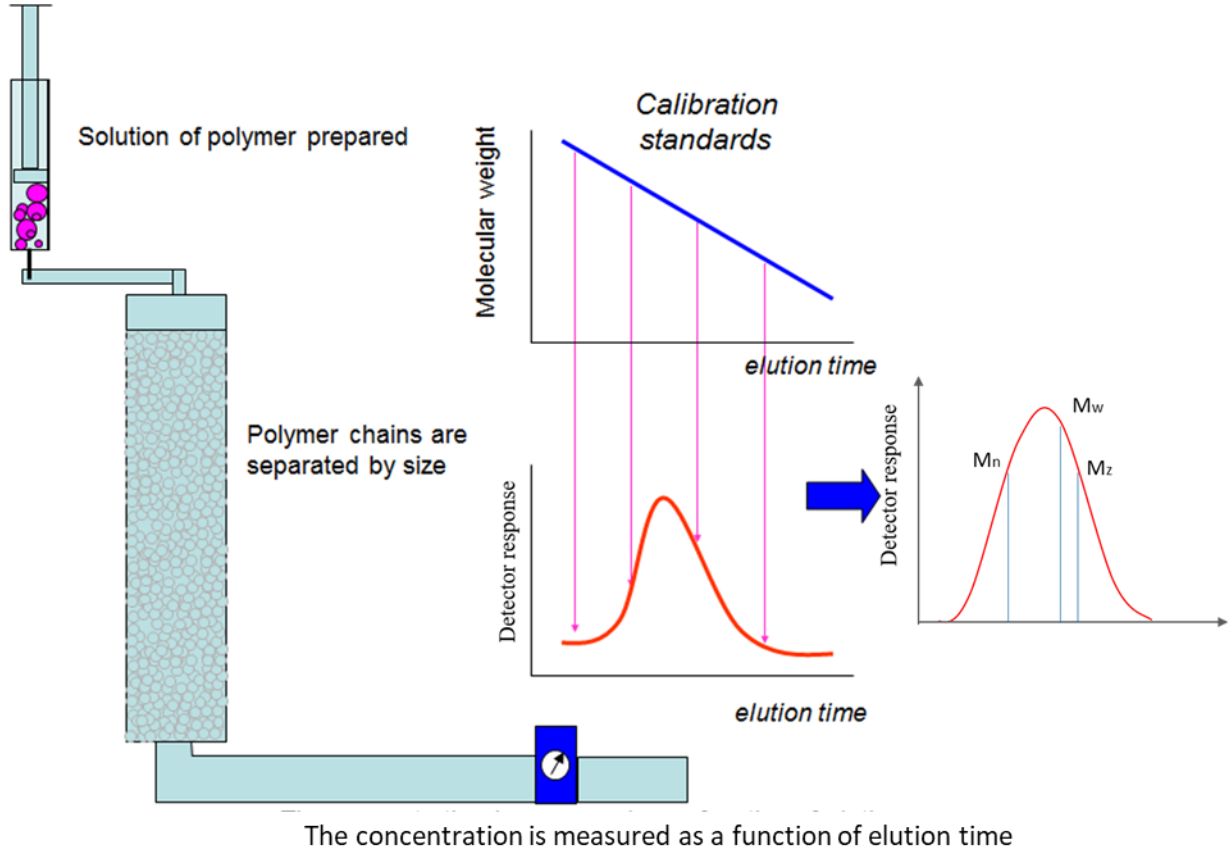

Figure 2-1 GPC schematic diagram.[18]

At the end of the column, one or a combination of detectors like refractive index (RI), infrared (IR), light scattering (LS), and viscosity detectors measure the mass concentration and other properties of the polymer in the flowing eluent.[20] A calibration curve, such as the one in Figure 2-2, relates the elution time to the molecular weight of the polymer of interest.[3] To create the calibration curve, polymer samples of known molecular weight and low PDI (calibration standards) are needed.

Benoit and coworkers showed that product $[\eta]$ M is a direct measure of the hydrodynamic volume of the molecules, where $[\eta]$ is the intrinsic viscosity of the polymer solution and M is the molecular weight of the polymer.[21] When the product $[\eta]$ M is plotted for a variety of polymers with narrow distribution, they all fall on the same curve, as shown in Figure 2-2,[3] thus eliminating the need of having standards of each polymer type that needs to be analyzed.

GPC columns are commonly calibrated using commercially available narrow-distribution polystyrene samples to relate the elution time (or elution volume) of the sample to its hydrodynamic volume. One of the benefits of having multiple detectors at the end of the column, such as a viscosity detector, is that the viscosity of the eluted sample can also be measured simultaneously which would lead to molecular weight measurement using the calibration curve.

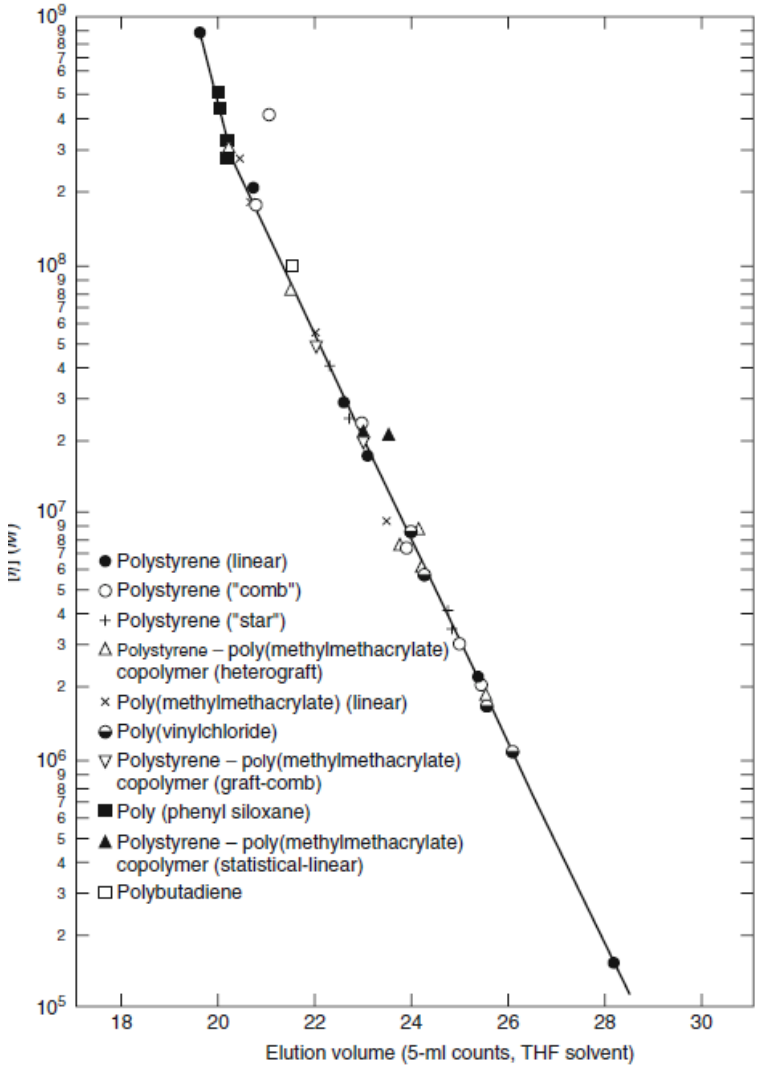

Figure 2-2 Universal calibration curve.[3]

2.1.1.1 Short Chain Branch Distribution

Short-chain branching has a large impact on the mechanical properties of polyethylene.[22] Moreover, short-chain branching across the molecular weight distribution also strongly influences the performance of polyethylene. For example, between two samples with similar M_n, MWD, and density, an ethylene/1-olefin copolymer with SCBs concentrated in the higher molecular weight chains has superior environmental stress crack resistance (ESCR) than a copolymer with more SCBs in the low molecular weight chains.[23] Short-chain branching (SCB) can be measured as a function of molecular weight with an IR or Fourier-transform infrared (FTIR) detector added at the end of the GPC column.

In GPC/IR or GPC/FTIR methods, the different molecular weight fractions of the analyte separated after eluting through the GPC columns, pass through a heated flow cell where they are subjected to IR radiation generating a series of IR spectra for different molecular weight fractions, similar to the one shown for diesel motor oil in Figure 2-3.23 The intensities of absorbance of these factions are measured in the 3000-2700 cm-1 band, as this corresponds to >C-H stretching region.24 Wavenumbers 2965 and 2928 cm-1 correspond to methyl (-CH3) and methylene groups (>CH2), respectively, and the ratio of the intensity of absorbance between methyl and methylene groups can be used to measure the SCB across different molecular weight fractions using a calibration curve (A2965(CH3)/ A2928(CH2)) ×SCB/1000C) constructed using polymers with known SCB frequency.

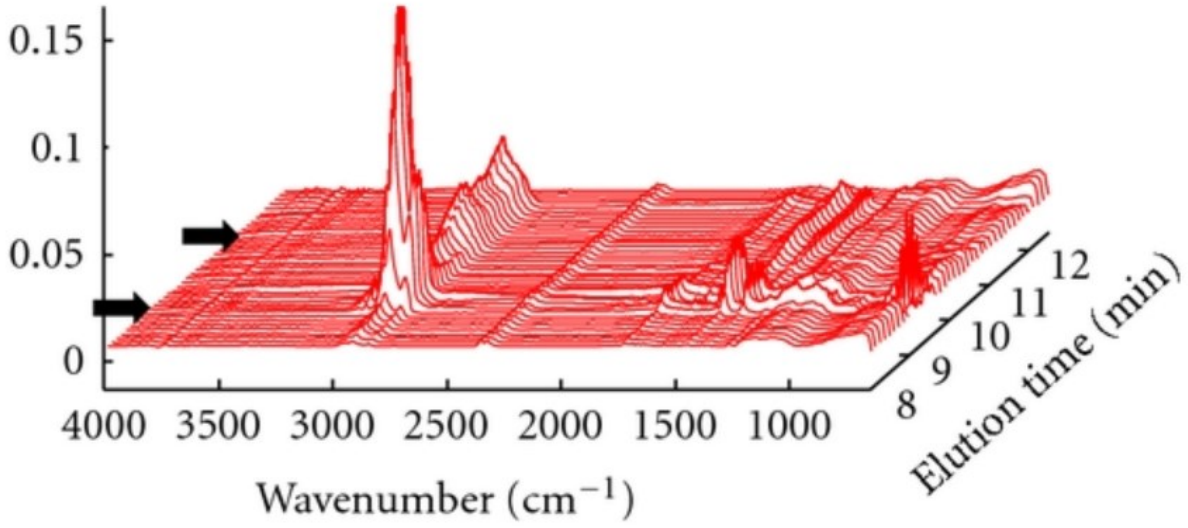

Figure 2-3 Time-ordered spectra from the GPCFTIR analysis of diesel motor oil.[24]

2.1.2 Differential Scanning Calorimetry

Differential scanning calorimetry is a technique used to study thermal transitions such as melting, crystallization, and glass transition of polymers and other materials. In this method, the polymer sample is kept in a pan (the sample pan) while the reference pan is kept empty. Both pans are heated at the same rate, usually 10 °C/minute. As the pans are heated, their temperatures begin to rise. The differential heat absorbed by the sample pan, owing to the presence of polymer sample, is recorded as a function of temperature, resulting in a plot similar to that shown in Figure 2-4.[25]

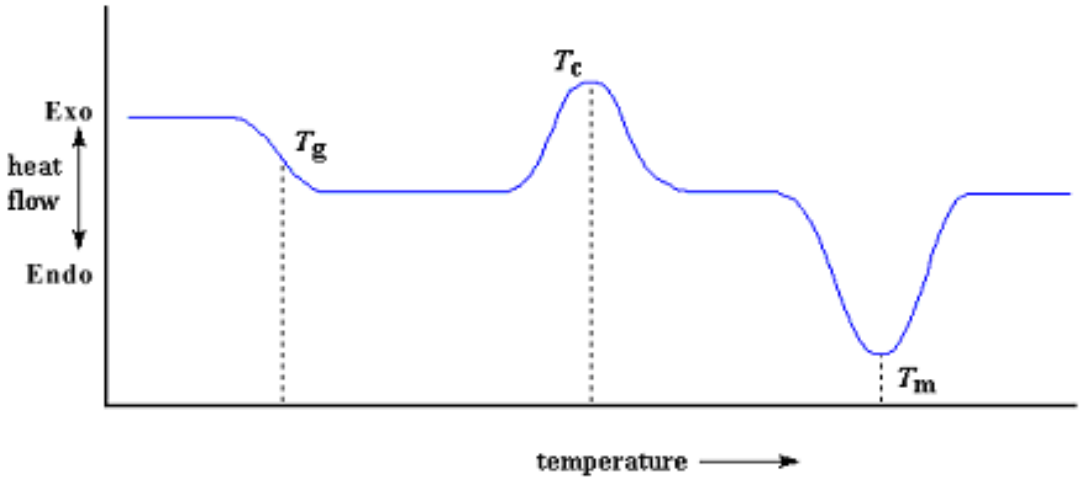

Figure 2-4 Typical DSC curve of a semi-crystalline polymer.[25]

As the polymer sample absorbs heat, it reaches a temperature called the glass transition temperature (T_g) where the polymeric chain segments gain energy to start long-range micro-Brownian motion.[26] Consequently, the heat capacity of the material increases, as shown by the transition in Figure 2-4. The phenomenon happens over a temperature range and not at a clear discreet value. Thus, the middle point of this range is taken to be the T_g. It is a critical parameter from a practical perspective as for numerous polymers, it decides the maximum operating temperature, while at the same time it also defines the lowest temperature at which it can be processed.[26]

Crystallization temperature (T_c) is defined as the temperature at which an isotropic liquid becomes a crystalline solid while cooling.[27] During crystallization, the chains arrange themselves into an ordered structure, thus, releasing energy in the process resulting in a rise in the curve. The peak of this rise is taken as crystallization temperature (T_c).

Heating the sample beyond the crystallization temperature (T_c) leads to melting. During melting, the crystalline ordered structure in the polymer breaks, and the chains start moving freely. It is an endothermic process; thus, heat is absorbed as shown in Figure 2-4. The peak of this curve is usually taken as the melting temperature (T_m) of the polymer. The melting temperature of the

copolymer can be related to comonomer incorporation for a variety of comonomers using a calibration curve. [28,29]

DSC can also be used to find out the degree of crystallinity of the sample. The heat absorbed by the sample during melting, heat of fusion, is normalized by the heat of fusion of a 100% crystalline sample of the same polymer to get the percent crystallinity where the latter is obtained from the values reported in the literature.[29]

2.1.3 Chemical Composition Distribution

The chemical composition distribution (CCD) is the second most important microstructural distribution of polyethylene. There are three crystallization-based techniques used for the estimation of CCD: temperature rising elution fractionation (TREF), crystallization analysis fractionation (CRYSTAF), and crystallization elution fractionation (CEF). In all three techniques, polymer chains are fractionated based on crystallizability: chains with low a-olefin content (more crystallizable) crystallize at a higher temperature, while those with high a-olefin content (less crystallizable) crystallize at a lower temperature; thus, chains can be fractionated from a dilute solution by decreasing the temperature slowly, in either a stirred vessel (CRYSTAF) or a packed column (TREF and CEF) as illustrated schematically in Figure 2.5.[3]

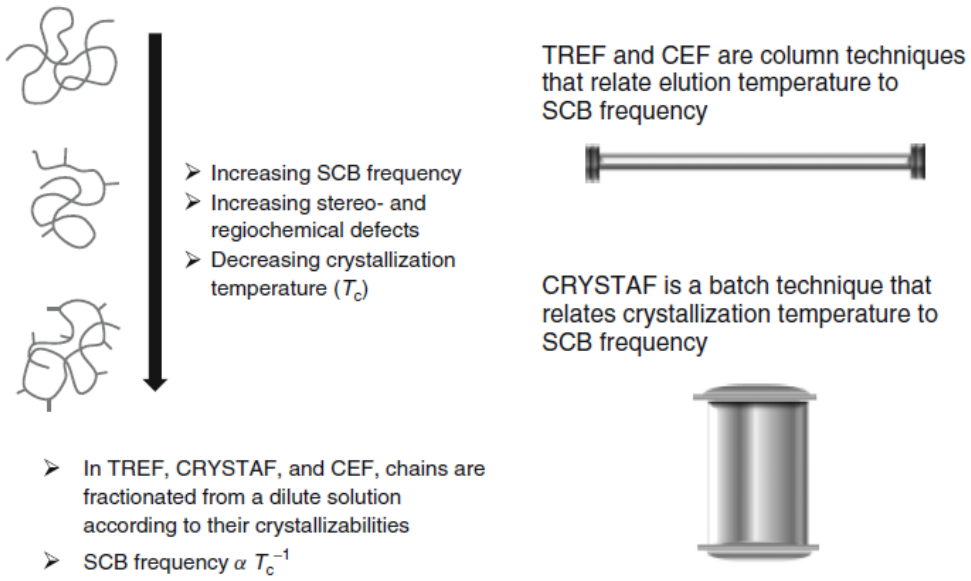

Figure 2-5 Fractionation techniques in CCD determination.[3]

TREF is the oldest of the 3 techniques. In this technique, a dilute polymer solution is transferred at high temperature to a column packed with inert beads. The beads provide the surface area for polymer chains to crystallize while the temperature is cooled down to the room temperature at a specified cooling rate; thus, the more crystallizable chains (higher crystallization temperature) crystallize first, followed by the less crystallizable chains (lower crystallization temperature). This is the end of the crystallization step.

Thereupon, a pure solvent is made to flow into the system while its temperature is increased. Less crystalline polymer chains dissolve in the solvent first and get eluted, followed by more crystalline chains, which are eluted subsequently. A mass detector measures the concentration of the polymer eluted at each temperature, as illustrated in Figure 2-6. A calibration curve is then used to convert the elution temperature to the mole fraction of the comonomer to estimate the CCD.[30]

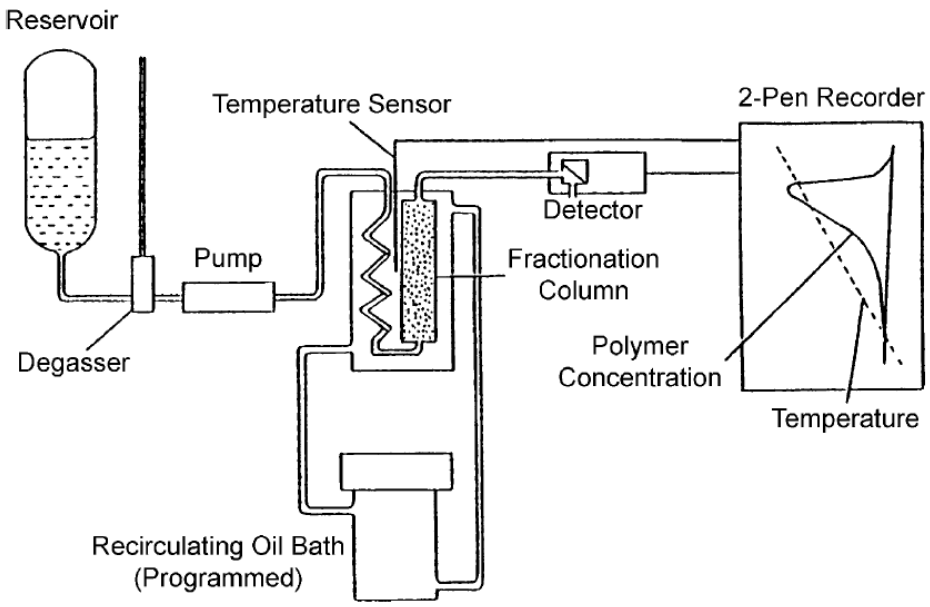

Figure 2-6 Schematic diagram of TREF.[30]

In CRYSTAF, stainless steel cylinders equipped with stirring units are placed inside a temperature-programmable oven. The sampling line is connected to a filter on one side, and an IR detector on the other to measure the polymer concentration as a function of crystallization temperature, as shown in Figure 2-7.[30]

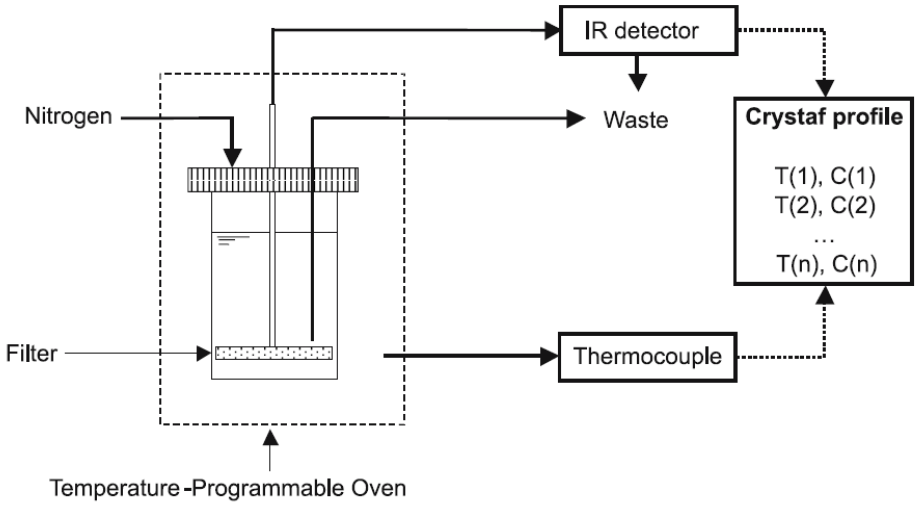

Figure 2-7 Schematic diagram of CRYSTAF.[30]

For analysis, the polymer is fully dissolved in a good solvent. The next step is the stabilization step where a temperature higher than the initial crystallization temperature is maintained while the solution is stirred, typically at the rate of 200 rpm. The stirring rate is dropped to 100 rpm during the subsequent step, the crystallization step, to ensure uniformity in polymer concentration distribution and to protect the filter from plugging.[30]

During the crystallization step, a uniform and slow cooling rate is maintained to allow chains with high crystallinity to precipitate out first, followed by chains with low crystallinity. As the chains begin to precipitate, a small aliquot of the residual polymer solution is pushed through the filter and collected by the sampling line to measure its corresponding crystallization temperature and polymer concentration using a thermocouple and the IR detector, respectively, generating a cumulative CRYSTAF profile similar to one shown in Figure 2-8.[31] The derivative of this cumulative CRYSTAF profile gives the relative amount of polymers crystallizing at each of the measured temperatures.

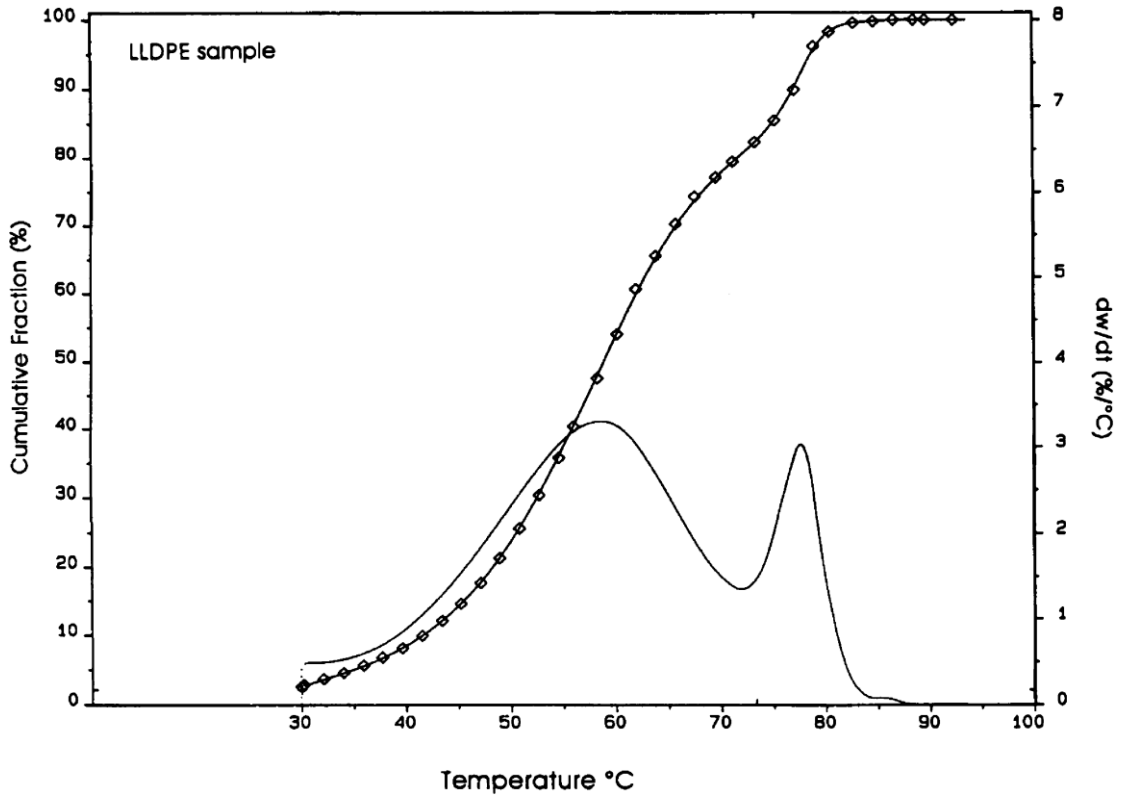

Figure 2-8 Typical cumulative and derivative CRYSTAF profile of an LLDPE sample [31]

Crystallization elution fractionation is a relatively new technique used for CCD analysis. Similar to TREF, a polymer solution is introduced in a column at high temperature and allowed to cool at a controlled rate; however, differently from TREF, the solvent is allowed to flow through the CEF column during the crystallization step. As the column is cooled, the chains with higher crystallizability crystallize first and get segregated on the support, while chains with lower crystallizability keep flowing through the column until they reach their own crystallization temperature. Thus, in the crystallization step of CEF, the polymer chains get spatially separated in the column according to their crystallizability. This step is followed by a temperature rising elution step at a different solvent flow rate which in turn, increases the separation further, as schematically presented in Figure 2-9.[32]

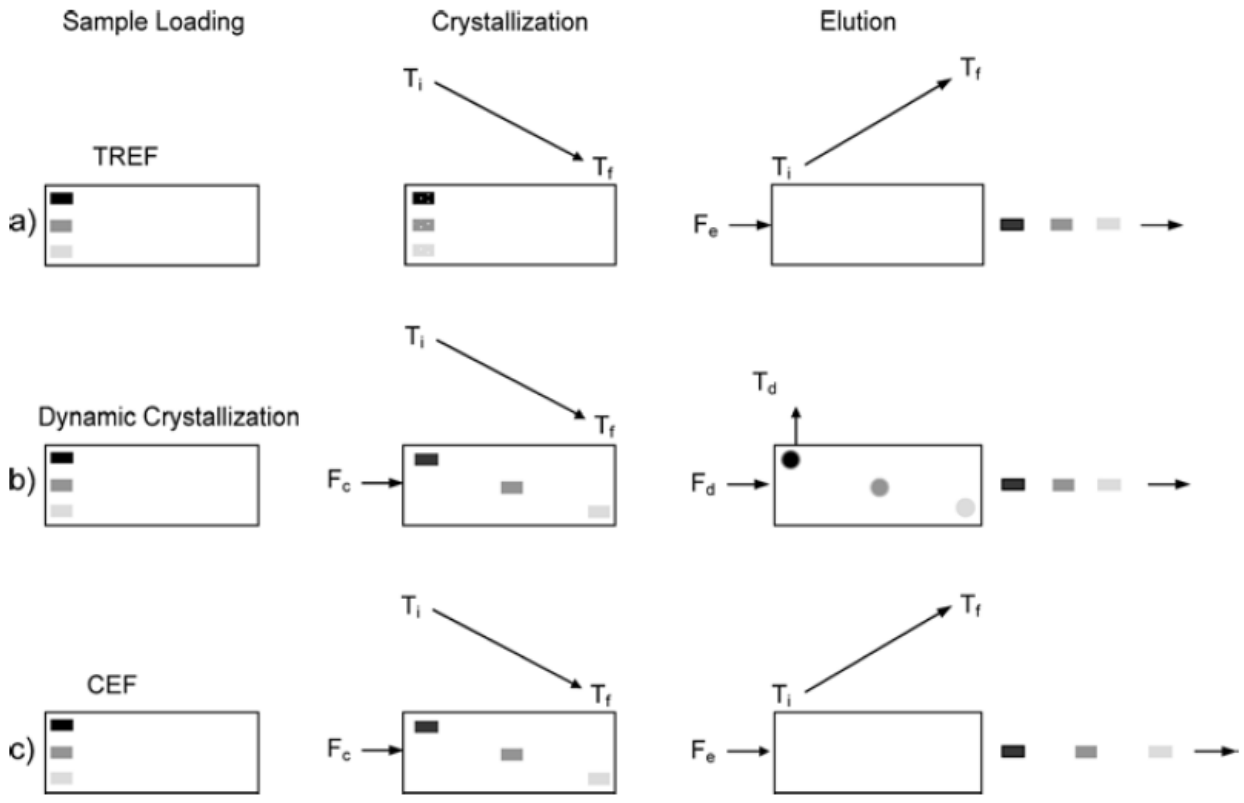

Figure 2-9 Separation technique in TREF, Dynamic Crystallization, and CEF.[32]

Figure 2-10 shows a CEF instrument diagram.[32] The polymer sample is usually dissolved in trichlorobenzene (TCB) and introduced in the column at a high temperature, where it is cooled at a controlled rate for crystallization to take place under a constant flow of solvent. After the crystallization step is complete, solvent at increasing temperature and higher flow rate is flown through the column, eluting polymer fractions to a dual-wavelength infrared detector to measure their concentrations and compositions.

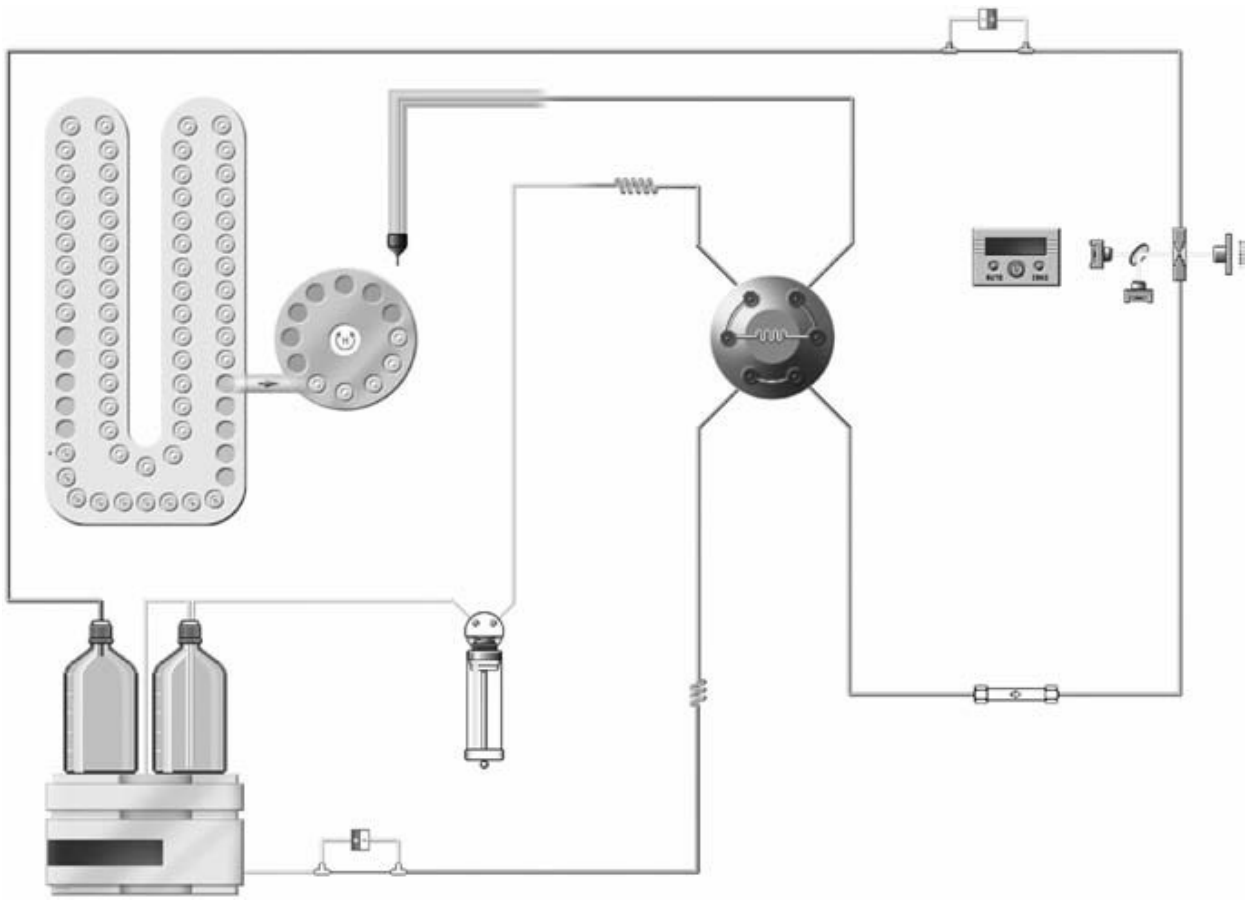

Figure 2-10 Schematic of CEF instrument diagram.[32]

2.2 Catalysts for Ethylene Polymerization

The first coordination catalytic system, Phillips Catalysts, was introduced by Phillips Petroleum Co. in 1951; the second by Ziegler and Natta, an invention for which they shared the Nobel Prize in Chemistry in 1963.[33]

Ziegler-Natta catalysts are composed of a transition metal salt of metals from groups IV to VII (Figure 2-11) and a metal alkyl of base metal from groups I to III, acting as an activator.[3] The catalysts discovered by Hogan and Banks (working for the Phillips Petroleum Co.) came to be known as Phillips catalysts, were chromium and molybdenum oxides supported on SiO_2 - Al_2O_3 (Figure 2-12).[3] Together these catalysts are used to produce 90% of the polyethylene in the world today, while the rest is made using metallocene catalysts.[11,34–36]

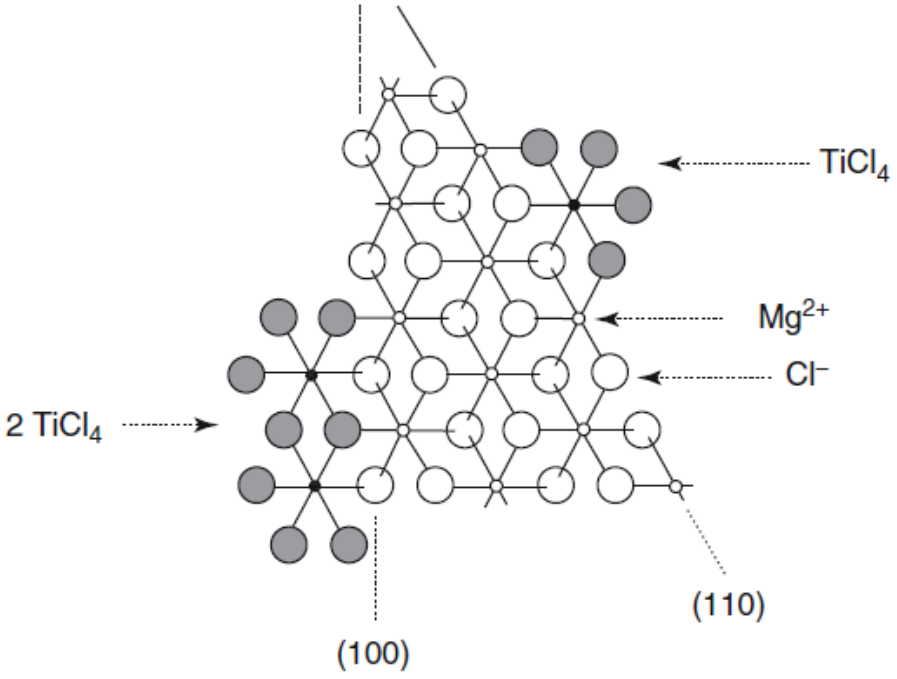

Figure 2-11 Structure of a generic $TiCl_4$/ $MgCl_2$ Ziegler-Natta catalyst.[3]

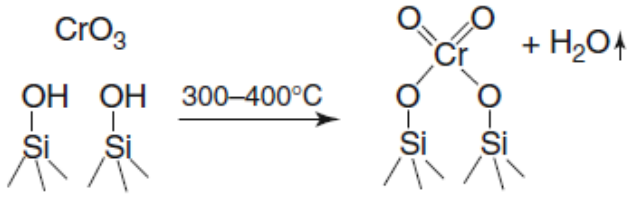

Figure 2-12 Structure of a chromium oxide Phillips catalyst.[3]

Polyolefins produced using Ziegler Natta and Phillips catalysts have non-uniform properties: broad MWD, non-uniform SCB frequency across the MWD, and broad CCD, as schematically shown in Figure 2-13 (a). Neither the MWD follows Flory distribution nor the CCD follows Stockmayer distribution, as would be expected for a polymer made with a single site catalyst under uniform polymerization conditions. This non-uniformity of properties mystified scientists since these catalysts started being used to make polyolefins. The picture became clearer with the discovery of another class of coordination catalyst, the metallocenes: the MWD and CCD of polyolefins made with metallocenes follow Flory and Stockmayer distributions, as illustrated in Figure 2-13 (b).

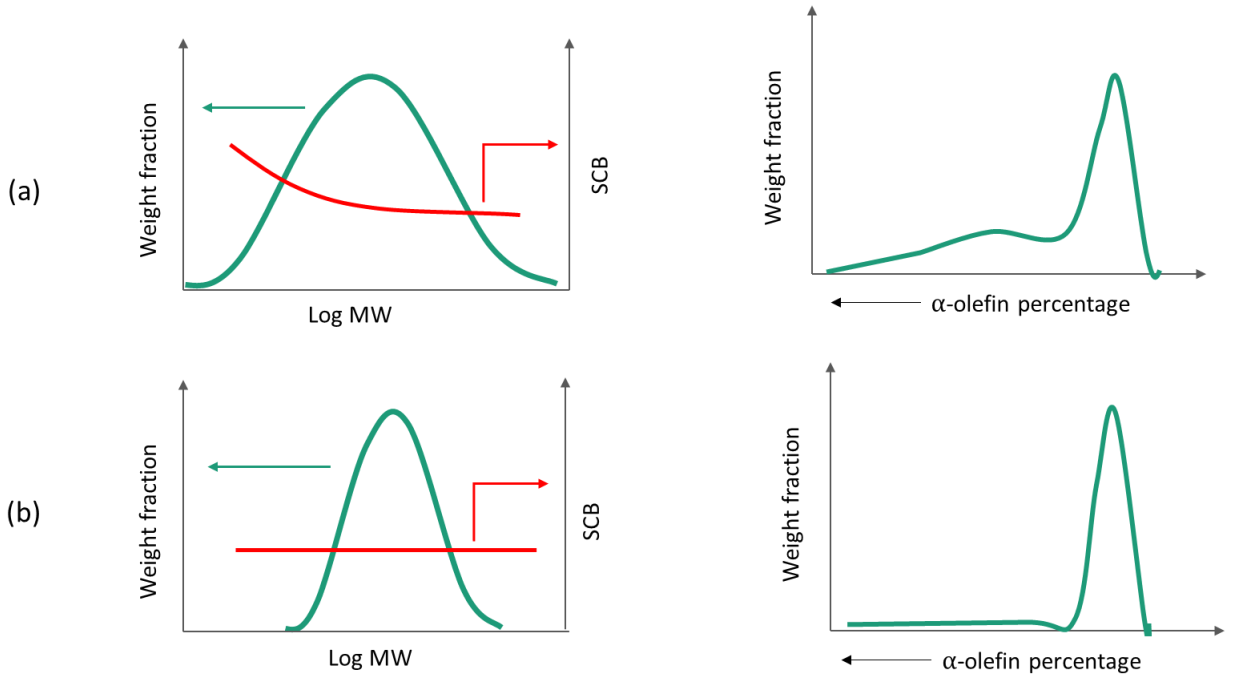

Figure 2-13 Schematic representation of MWD, SCBD, and CCD of polymers produced using: (a) Ziegler-Natta or Phillips, and (b) metallocene catalysts.

The unexpected properties of polymers produced with Zeigler-Natta catalysts is attributed to the presence of the multiple site types, as schematically illustrated in Figure 2-14 (a). Each site type has a distinct set of polymerization kinetic constants and behaving like a single site catalyst, producing polymers whose MWD and CCD are narrow and uniform.[36–38] The overall broad

microstructure is envisioned to be a blend of the narrower polymer populations produced on each site type, as illustrated in Figure 2-14 (b). This concept formed the basis for the development of many mathematical modeling approaches for the microstructure of the polymers produced using Zeigler-Natta and Phillips catalysts, as detailed in the next section.[12–15,36–38,39]

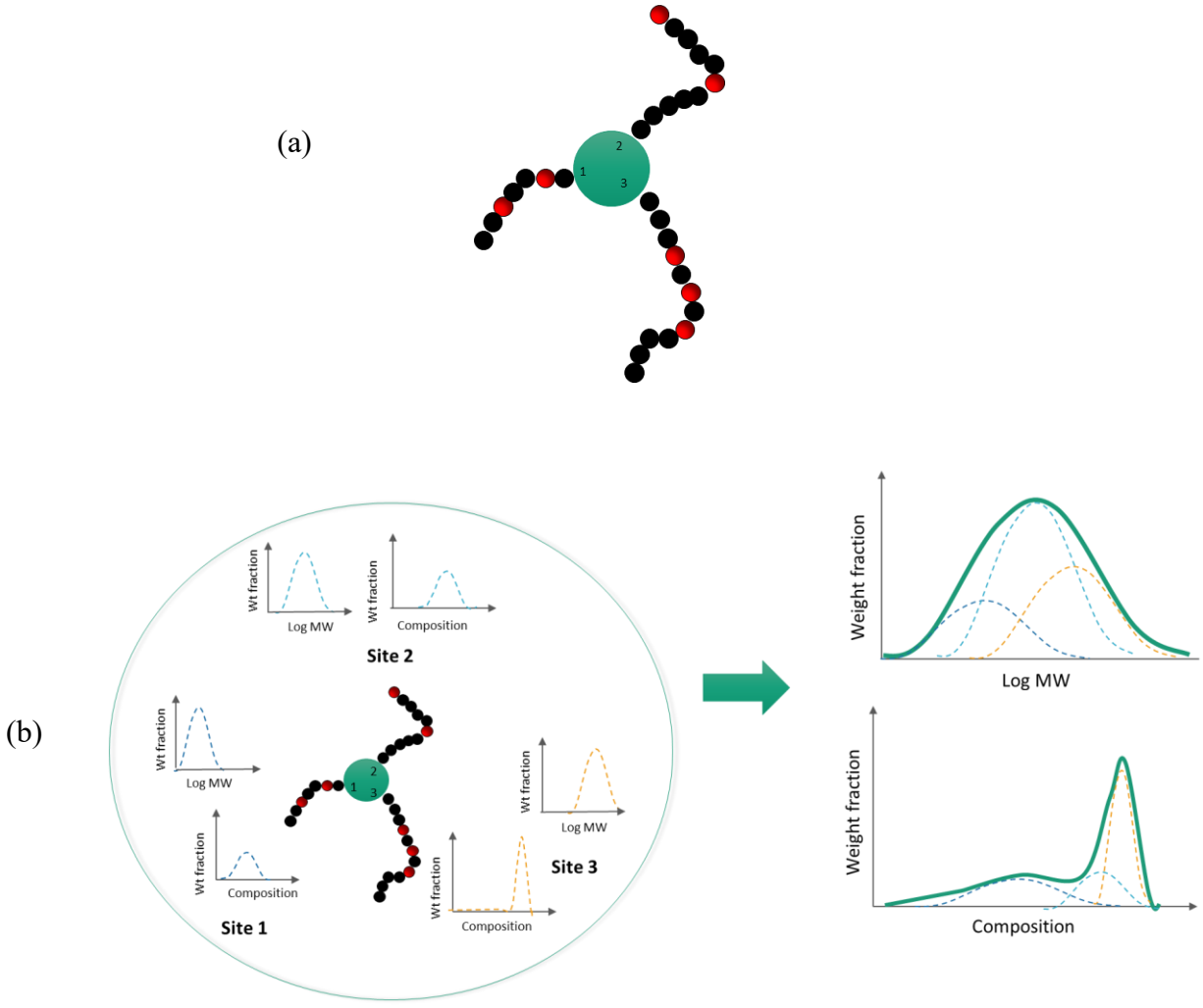

Figure 2-14 (a) Schematic illustration of multi-site nature of the Ziegler Natta catalysts, (b) effect of multi-site nature of the Ziegler Natta catalysts on polymer microstructure.

Metallocene catalysts, as shown in Figure 2-15, were discovered in 1957 independently by Natta and Breslow, who used them to polymerize olefins using Al alkyl co-catalysts.[3] However, these

catalyst systems were unstable and had poor polymerization rates. In 1980, Kaminsky and Sinn discovered that methyl aluminoxane (MAO) could be used as a cocatalyst to activate and stabilize metallocene catalyst systems. This generated a lot of interest in these catalyst systems owing to their high activity as well as stability. These were the first catalysts to be truly single site in nature; as a result, the polymers made using them had uniform properties, with narrow MWD and CCD, as well as uniform comonomer composition across the MWD (Figure 2-13 (b)).

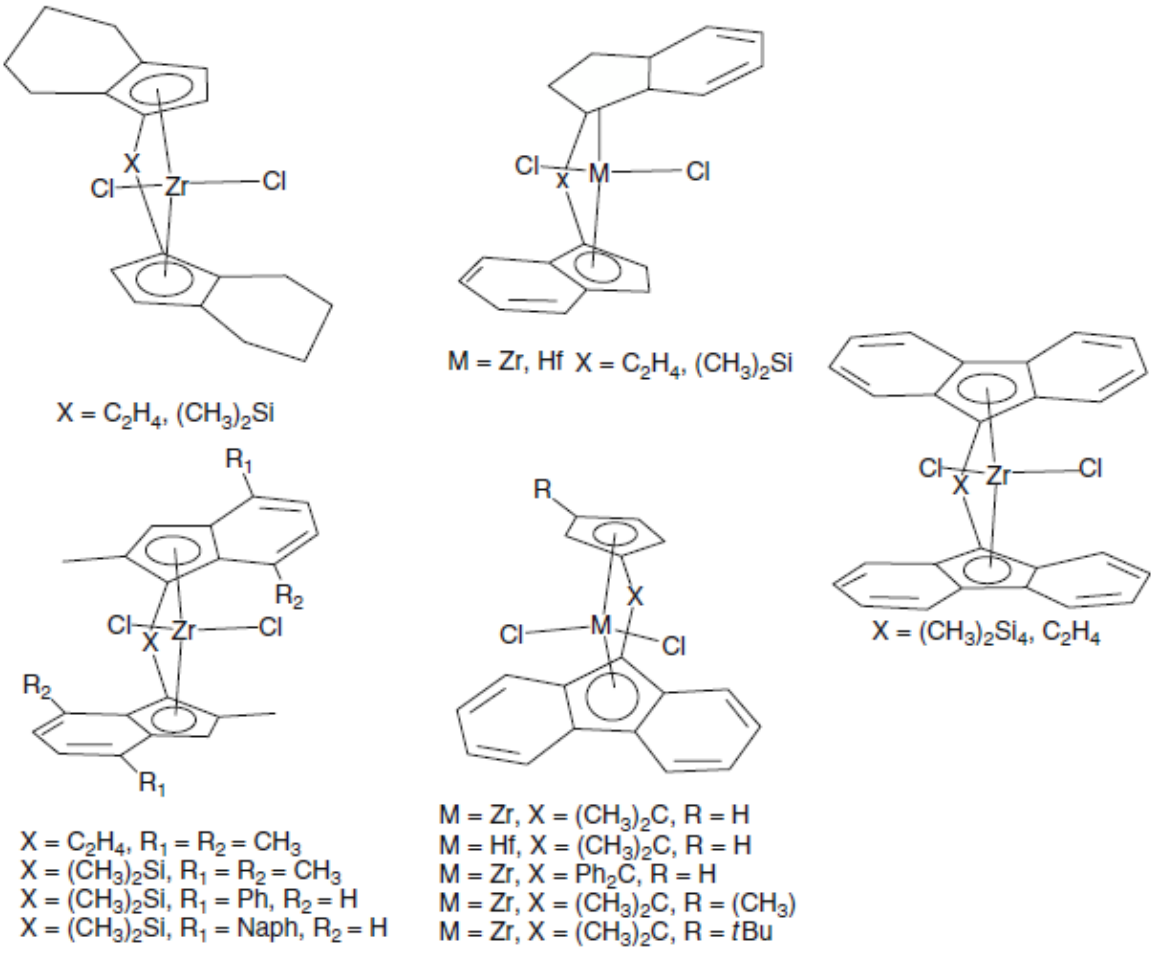

Figure 2-15 Structure of a few different metallocene catalysts.[3]

Late transition metal catalysts were first developed in 1991 by Brookhart and co-workers. Their higher electronic density and bulky chelated ligands gave them more stability and capability of polymerization of monomers with different functional groups.[40]

Table 2-1 summarizes the four main classes of coordination catalysts used for olefin polymerization, their physical states, a few examples, and the nature of microstructural properties of the polymers they make.[3]

Table 2-1 Four major classes of coordination catalysts and their characteristic properties. [3]

Type	Physical state	Examples[a]	Polymer type
Ziegler–Natta	Heterogeneous	$TiCl_3$, $TiCl_4/MgCl_2$	Nonuniform
	Homogeneous	VCl_4, $VOCl_3$	Uniform
Phillips	Heterogeneous	CrO_3/SiO_2	Nonuniform
Metallocene	Homogeneous	Cp_2ZrCl_2	Uniform
	Heterogeneous	Cp_2ZrCl_2/SiO_2	Uniform
Late transition metal	Homogeneous	Ni, Pd, Co, Fe with diimine and other ligands	Uniform

2.3 Polyolefin Microstructural Modeling

Polyolefin microstructural distributions (MWD, CCD, and SCBD) dictate their final applications. In the following sections, mathematical models describing these polyolefin microstructures are discussed.

2.3.1 Single-Site Models

The joint MWD and CCD of polymers with kinetic chain length (r) and molar fraction of monomer type A (F_A) produced by a single site catalyst follows Stockmayer bivariate distribution.[40]

For linear binary copolymers, it is expressed as follows,

$$w\,(r, F_A) = r\ \times\ \tau^2 \times exp(-r \times \tau) \times \frac{1}{\sqrt{2\pi\beta/r}} \times exp\left[-\frac{(F_A - \bar{F}_A)^2}{2\beta/r}\right] \tag{2.3}$$

$$\beta = \bar{F}_A(1 - \bar{F}_A)\ \times \sqrt{1\ + 4 \times \bar{F}_A(1 - \bar{F}_A)(r_A \times r_B - 1)} \tag{2.4}$$

where τ is the ratio of the sum of all transfer rates to the propagation rate, $\bar{F}_A$ is the average mole fraction of monomer type A in the copolymer, and $\mathrm{r_A}$ and $\mathrm{r_B}$ are the copolymerization reactivity ratios. The number average chain length is given by $1/\tau$. Therefore, the number average molecular weight (M_n) can be calculated as $M_n = mw/\tau$, where mw is the average molecular mass of the repeating unit in the copolymer chains.

The MWD component of Stockmayer distribution, Flory most probable distribution, is obtained by integrating Stockmayer distribution overall chemical compositions,

$$w\,(r) = r\ \times\ \tau^2 \times exp(-r \times \tau) \tag{2.5}$$

Flory distribution is often represented in logarithmic scale, as it is the usual way to report MWDs measured by gel permeation chromatography (GPC).

$$w_{log\,r} = 2.3026 \times r^2\tau^2 exp\,(-r\tau) \tag{2.6}$$

To get the MWD, we change the number average chain length r_n, by the number average molecular weight, M_n, and r is replaced by the molecular weight of the polymer chain, $MW = r \times mw$, where mw is the average molar mass of the repeating unit in the polymer chain. Using the transformations, we now have the MWD as,

$$w_{MW} = \frac{MW}{{M_n}^2} exp\left(\frac{-MW}{M_n}\right) = MW\hat{\tau}^2 exp\,(-MW\hat{\tau}\,) \tag{2.7}$$

and the parameter $\hat{\tau}$ is defined as

$$\hat{\tau} = \frac{1}{M_n} = \frac{1}{r_n mw} = \frac{\tau}{mw} \tag{2.8}$$

Equation (2.6) in logarithmic scale can be written as,

$$w_{log\,MW} = 2.3026 \times MW^2\hat{\tau}^2 exp\,(-MW\hat{\tau}\,) \tag{2.9}$$

Similarly, the CCD component of Stockmayer distribution is calculated by integrating Stockmayer distribution over all the chain lengths as,

$$w\,(F_A) = \frac{3}{4\sqrt{2\beta\tau}\left[1 + \frac{(F_A - \bar{F}_A)^2}{2\beta\tau}\right]^{\frac{5}{2}}} \tag{2.10}$$

For copolymer chains made on each site type, the average mole fractions of monomer type 1 are statistically independent of the kinetic chain length; long chains and short chains have the same average chemical composition.[41]

2.3.2 Multiple-Site Model

The microstructure of polymers made with multiple-site type catalysts, such as the Ziegler-Natta catalysts, can be modeled as a weighted average of the microstructures of the chain populations made on each site type. Therefore, the bivariate MWD×CCD can be calculated from a superposition of Stockmayer distributions as

$$w(r, F_A) = \sum_{j=1}^{n} m_j \, w_j(r, F_A) \tag{2.11}$$

where n is the number of site types, m_j is the mass fraction of polymer made on-site type j, and $w_j(r, F_A)$ is the Stockmayer distribution of polymers made on-site type j.

Similarly, the MWD and CCD of polymers synthesized with multiple-site-type catalysts in log form are given by

$$w(r) = \sum_{j=1}^{n} m_j \, w_j(r) \tag{2.12}$$

$$w(log\, MW) = \sum_{j=1}^{n} m_j (2.3026 \times MW_i{}^2 \hat{t}_j{}^2 \, exp(-MW_i \hat{t}_j{}^2)) \tag{2.13}$$

$$w(F_A) = \sum_{j=1}^{n} m_j \, w_j(F_A) \tag{2.14}$$

$$w\,(F_A) = \sum_{j=1}^{n} m_j \frac{3}{4\sqrt{2\,\beta_j \tau_j}\left[1 + \frac{(F_A - \bar{F}_{Aj})^2}{2\beta_j \tau_j}\right]^{\frac{5}{2}}} \tag{2.15}$$

where $w_{\log MWj}$ and $w_{F_{Aj}}$ are the MWD and CCD of copolymers made on-site type j, respectively, as given by Equation (2.9) and Equation (2.10).

For copolymer chains made with multiple-site-type catalysts in which each site type produces copolymer chains with different average comonomer fractions, the average mole fractions of monomer type A as a function of the kinetic chain length can be calculated with the following equation

$$F_A(r) = \frac{\sum_{j=1}^{n} m_j \, w_j(r) \, \bar{F}_{A,j}}{\sum_{j=1}^{n} m_j \, w_j(r)} \tag{2.16}$$

where $\bar{F}_{A,j}$ is the average mole fraction of monomer type A made on site type j.

When the copolymers are analyzed using GPC-IR, we get the MWD and SCBD. The average comonomer composition is given by

$$SCB\,(r) = \frac{\sum_{j=1}^{n} m_j \, w_j(r) \, \overline{SCB}_j}{\sum_{j=1}^{n} m_j \, w_j(r)} \tag{2.17}$$

Chapter 3
Copolymer Synthesis and Characterization

3.1 Introduction

Copolymers of ethylene and 1-hexene were synthesized with Zeigler-Natta and metallocene catalysts in a stainless-steel autoclave reactor operated in semi-batch mode. The polymerization procedure details are given in the next section.

Gel permeation chromatography with infrared detector (GPC-IR) was used to determine molecular weight distributions (MWD) and short-chain branching distribution (SCBD) across the molecular weight of these samples. The chemical composition distributions (CCD) of these samples were measured with crystallization elution fractionation (CEF).

3.2 Copolymer Sample Synthesis

3.2.1 Materials

The materials used to make ethylene/1-hexene copolymers were toluene, ethanol, ethylene, 1-hexene, methylaluminoxane (MAO), nitrogen, triisobuylaluminum (TIBA), trimethylaluminum (TEA), hydrogen, a Ziegler–Natta catalyst ($TiCl_4$ /$MgCl_2$), metallocene catalysts (methyl (6-t-butoxyhexyl) silyl (η5-tetramethylcyclopentadienyl) (t-butylamido) titanium dichloride (CGC-Ti), and bis(cyclopentadienyl) hafnium (IV) dichloride). 1,2,4-Trichlorobenzene was used to make solutions for copolymer characterization. Table 3-1 shows the detailed information for these materials.

Table 3-1 Materials used in the synthesis and characterization of ethylene/1-hexene copolymers

Material	Supplier	Purity
Toluene	Sigma-Aldrich	99.9% for HPLC
Ethanol	Sigma-Aldrich	For HPLC
1-hexene	Sigma-Aldrich	97%
TIBA	Sigma-Aldrich	25 wt% in toluene
TEA	Sigma-Aldrich	25 wt% in toluene
TCB	Sigma-Aldrich	For GPC and CEF
MAO	Albemarle	10 wt% in toluene
Nitrogen	Praxair	99.9980%
Ethylene	Praxair	99%
Hydrogen	Praxair	99.95%
CGC-Ti	LG Chem	0.428 M (dissolved in toluene)
$TiCl_4$ /$MgCl_2$ Ziegler–Natta catalyst		1.3 wt%
Bis(cyclopentadienyl) hafnium (IV) dichloride	Sigma-Aldrich	97%

3.2.2 Polymerization Procedure

All polymerizations were performed in a 300-ml Parr autoclave reactor operated in semi-batch mode. Before being injected into the reactor, ethylene was flown through molecular sieves (3A/4A mixture) and a copper (II) oxide bed to remove polar impurities. The catalyst (Ziegler-Natta catalyst suspension or metallocene solution, both in toluene), co-catalyst, and 1-hexene were transferred to 20 ml vials and sealed with rubber caps and metal crimps inside a glove box under an inert N_2 environment. The sealed vials were removed from the glove box and transferred to the reactor through flexible stainless-steel needles to avoid air contamination. Figure 4-1 shows the P&ID diagram of the setup. [42]

At the beginning of each polymerization, the reactor was washed with 150 ml toluene and 0.5 g of TIBA (used as a scavenger) and heated to 140 °C. After keeping the reactor at 140 ºC for 10 min, the toluene-TIBA mixture was removed under N_2 pressure. After washing with toluene, the reactor was purged with N_2 six times to remove any further impurities left in the system. Finally, the reactor was cooled to 40 °C to charge the solvent and reaction mixture to the system.

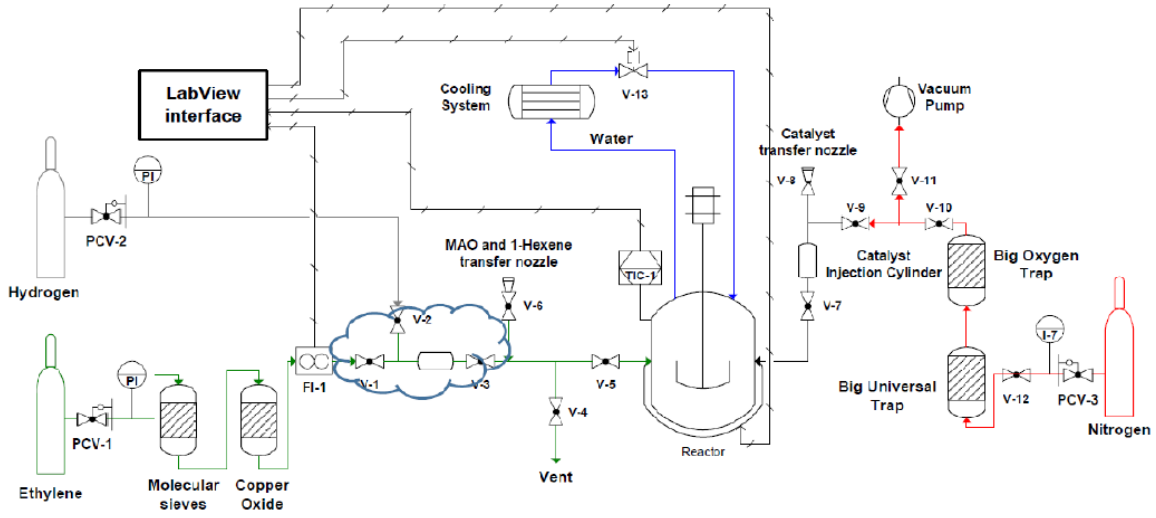

Figure 3-1 P&ID diagram of the reactor system.[42]

The Al/Ti was kept around 400 when using $TiCl_4/MgCl_2$ and MAO. While the Al/catalyst ratio was higher than 24,000 when using the metallocene catalysts, CGC-Ti, and Cp_2HfCl_2, to suppress the formation of LCBs.[43] The desired amounts of cocatalyst — TEA in case of Ziegler-Natta catalysts and MAO in case of metallocenes —1-hexene, and 150 ml of toluene were transferred to the reactor. The amount of 1-hexene controlled the degree of SCB in the copolymers. Subsequently, the desired volume of H_2 was transferred using a 30 mL volumetric bomb. The H_2 pressure was manipulated to control the mass of H_2 transferred to the reactor and, in turn, regulate the molecular weight of the copolymer. Finally, the ethylene line was connected to the H_2 bomb. The pressure from the ethylene line ensured the complete transfer of H_2 into the reactor. The ethylene and H_2 pressure were varied in the polymerization reactions to achieve the

desired polymer molecular weight. The catalyst (a Ziegler-Natta catalyst suspension of a metallocene solution in 10 ml of toluene) was first injected into a bomb connected to the reactor and then injected into the reactor using N_2 at a pressure higher than the ethylene pressure to start the polymerization. The polymerization mixture was stirred at 1300 rpm.

The polymerization temperatures were also varied to achieve the desired polymer molecular weight. The temperature for the Ziegler-Natta polymerizations was kept below 90°C (slurry polymerization) but higher above 105 °C for metallocenes (solution polymerization). A LabVIEW program was used to maintain the desired reactor temperature using an external electrical heating mantle and a cooling coil connected to a water bath by varying the output to the mantle and water flow rate to the cooling coil.

After the desired amount of polymer was synthesized (about 5 g per run), as estimated using the LabVIEW program concurrently during the polymerization, the reactor stirrer was stopped and the polymer was collected. For ZN Polymers, the reactor was cooled to room temperature and the polymer was slurry was collected after disassembling the reactor. For metallocene polymers, the polymer solution was purged out of the reactor under N_2 pressure. The polymer was then precipitated in 150 to 200 ml of ethanol, filtered, and dried in an oven at 70 °C overnight.

3.3 Copolymer Characterization

3.3.1 Gel Permeation Chromatography

Gel permeation chromatography, also known as size exclusion chromatography (SEC), was used to measure the molecular weight distribution (MWD) of the polyolefin samples. Our GPC unit (Polymer Char, Valencia, Spain) contained three linear columns filled with porous packing material (Agilent PLgel Olexis, 7.5×300 mm, 13 μm particles) and three detectors: infrared (IR), light scattering, and differential viscometer. Trichlorobenzene (TCB) was used as a solvent and continuous phase. All analyses were done at 145 °C at a TCB flow rate of 1.0 ml/min.

The GPC was calibrated (by Dr. S. Mehdiabadi) using narrow MWD polystyrene standards and the universal calibration curve. The online IR detector of the GPC unit was also used to measure the fraction of 1-hexene across the MWD. This signal was calibrated using ethylene/1-hexene copolymer standards of known chemical composition and polystyrene standards.

The IR detector in the GPC unit acted as a mass and a composition detector by recording the CH_2 and CH_3 frequencies of the polymer chains eluting the column set. The CH_2 signal was proportional to the mass of polymer, while the CH_3/CH_2 signal ratio was used to measure the SCB frequency, which was converted to the 1-hexene molar fraction in the copolymer, F_B, using the expression,

$$F_B = \frac{2 \times SCB}{1000 + (2 - n_c) \times SCB} \tag{3.1}$$

where n_c is the number of carbon atoms in the 1-hexene (6 for 1-hexene, for instance) and SCB is the number of short-chain branches per 1000 carbon atoms in the chain.

3.3.2 Crystallization Elution Fractionation

Crystallization elution fractionation (CEF) was performed using a CEF instrument from Polymer Char. The samples were prepared in TCB stabilized with 300 ppm of 2,6-di-tert-butyl-4-methyl phenol, at a concentration of 1 mg/mL. The volume of the injected sample was 200 μL. The polymer solution was stabilized at 110 °C for 12 min before being injected into the CEF column. The cooling cycle started by decreasing the column temperature from 110 to 35 °C under a constant cooling rate of 1 °C/min and a constant crystallization flow rate of 0.03 mL/min. At the end of the cooling cycle, the column temperature was held at 35 °C for 2 min under a constant elution flow rate of 0.5 mL/min. The elution cycle started with a heating rate of 2 °C/min and temperature changing from 35 to 160 °C. The concentration of polymer in the eluent was monitored as a function of the elution temperature by a dual-wavelength infrared detector placed at the exit of the CEF column.

Chapter 4
Results and Discussion

4.1 Introduction

The objective of the thesis was to validate the numerical deconvolution techniques for MWD and CCD of polyolefins made with Ziegler-Natta catalysts. The MWD and CCD are measured in two different instruments, GPC and CEF, respectively. The average short chain branching frequency across the MWD (which we are calling SCBD in this thesis) can be measured simultaneously with the MWD using a GPC-IR set up. In principle, if we could get all information needed by deconvoluting the MWD–SCBD using a single GPC-IR analysis, we would not need to analyze the CCD using CEF. Therefore, the first thing to do is to answer the question: Can MWD–SCBD deconvolution eliminate the need for CCD deconvolution?

An ethylene/1-hexene copolymer was synthesized with a commercial $TiCl_4$ /$MgCl_2$ Ziegler–Natta catalyst and their MWD-SCBD measured by GPC-IR were deconvoluted to determine the properties of the polymer populations made on each different site type. The polymers identified for these individual populations were then synthesized using a single-site metallocene catalyst (CGC-Ti or bis(cyclopentadienyl) hafnium (IV) dichloride) and blended in the proportions determined by the deconvolution procedure to find out whether this blend had the same MWD-SCBD of the polymer made with the Ziegler–Natta catalyst. Moreover, the CCDs of the Ziegler-Natta polymer and its equivalent metallocene polyolefin blend were also analyzed by CEF. These CCDs were then compared to find out whether they agreed or not.

4.2 Microstructure of the Ethylene/1-Hexene Copolymer Made with the Ziegler-Natta Catalyst

We first made a copolymer of ethylene and 1-hexene using a commercial Ziegler-Natta catalyst and analyzed it using GPC-IR and CEF, as described in Chapter 3. The synthesis conditions for

this resin are described in Appendix A. The results of these analyses are shown in Figure 4-1 and the microstructural parameters are listed in Table 4-1. The polydispersity index was greater than 2 and the SCB frequency was higher for the low molecular weight polymer populations and decreased progressively as the polymer molecular weight increased. Finally, the CCD was broad, bimodal, and non-uniform. These microstructural characteristics are typical of copolymers made with Ziegler-Natta catalysts. From this point onwards, we will call this sample the *ZN polymer*.

(a)

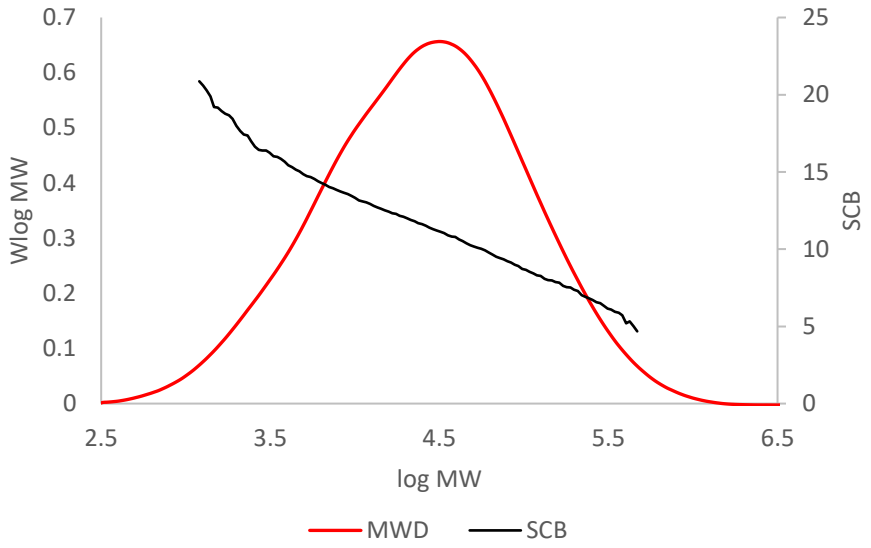

(b)

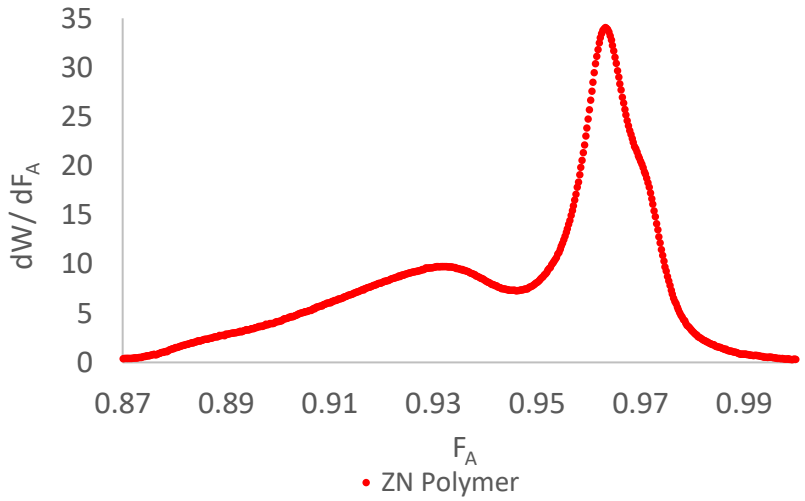

Figure 4-1 (a) MWD–SCBD, (b) CCD (converted from the elution temperature profile from CEF) of the ethylene/1-hexene copolymer made using a commercial Ziegler-Natta catalyst (ZN polymer).

Table 4-1 Microstructural parameters of the ethylene/1-hexene copolymer made using a commercial Ziegler-Natta catalyst (ZN polymer).

M_n	M_w	PDI	$\overline{SCB}$	Peak Elution Temperature (°C)	1-Hexene Mole Fraction, $\bar{F}_B$
9,900	58,000	5.9	11.8	83.3	0.022

Crystallization elution fractionation (CEF) measures the elution temperature profile of polyolefins, as explained in Section 2.1.3. The CCD is estimated from the temperature profile using a linear calibration curve that relates elution temperature to ethylene mole fraction, F_A. Figure 4-2 explains this procedure.

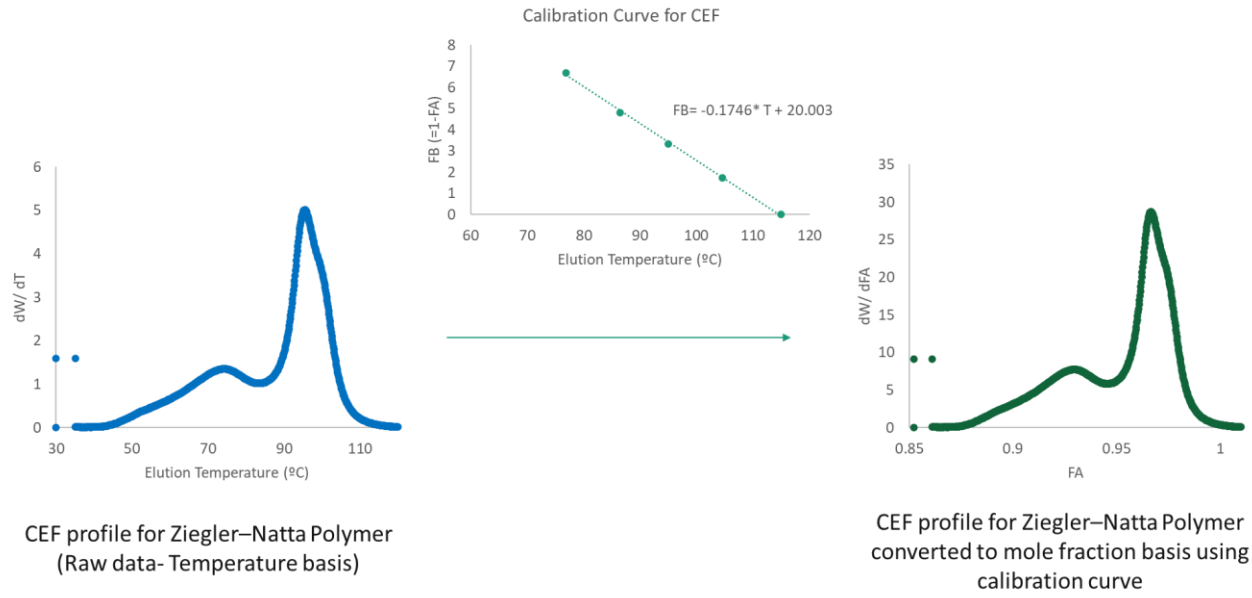

Figure 4-2 How to convert a CEF temperature profile to the equivalent CCD using a calibration curve.

4.3 MWD and SCBD Deconvolution

The MWD of the ZN polymer was deconvoluted following the standard curve-fitting approach[13,44] using the equation,

$$w_{\log M} = \sum_{j=1}^{n} m_j (2.3026 \times {M_i}^2 {\hat{\tau}_j}^2 \exp(-M_i {\hat{\tau}_j}^2)) \quad (4.1)$$

The minimum number of Flory distributions needed to describe the experimental MWD is obtained by minimizing the objective function,

$${\chi_1}^2 = \sum_{i=1}^{n_{GPC}} (w_{\log M,i}^{\mathrm{GPC}} - w_{\log M,i})^2 \quad (4.2)$$

$${\chi_1}^2 = \sum_{i=1}^{n_{GPC}} [w_{\log M,i}^{\mathrm{GPC}} - \sum_{j=1}^{n} m_j (2.3026 \times {M_i}^2 {\hat{\tau}_j}^2 \exp(-M_i \hat{\tau}_j))]^2 \quad (4.3)$$

where n_{GPC} *i*s the number of data points in the GPC distribution of the ZN polymer, $w_{\log M}^{GPC}$, and ${\chi_1}^2$ is the sum of the squares of the differences between the experimental data points and model predictions. Non-linear least-squares optimization was used to find the number of site types, n, mass fractions of polymer populations made on site type *j*, m_j, and $\hat{\tau}_j$ by estimating 2 × n-1 parameters (since, $\sum m_j = 1$). We started with assuming the minimum number of sites to be 3 and kept increasing the number of site types until the value of ${\chi_1}^2$ did not decrease anymore.

The SCBD deconvolution was performed after the MWD deconvolution.[45] The average SCB per site type was then determined by minimizing the objective function ${\chi_2}^2$,

$${\chi_2}^2 = \sum_{i=1}^{n_{GPC-IR}} (SCB_{exp,i} - SCB_{model,i})^2 \quad (4.4)$$

$${\chi_2}^2 = \sum_{i=1}^{n_{GPC-IR}} \left(SCB_{exp,i} - \frac{\sum_{j=1}^{n} m_j w_{i,j} \overline{SCB}_j}{\sum_{j=1}^{n} m_j w_{i,j}} \right)^2 \quad (4.5)$$

where n_{GPC-IR} is the number of data points collected by the GPC-IR detector, $\overline{SCB}_j$ is the average SCB/1000 C for site type j, m_j is the mass fraction of polymer made on site type j, and $w_{i,j}$ is the value of the Flory distribution for site type j for the weight corresponding to GPC-IR sampling point i.

The MWD–SCBD deconvolution results for the ZN polymer are shown in Figure 4-3. The fits for MWD and SCBD are excellent. The parameters estimated with this procedure are listed in Table 4-2. The next step in the proposed procedure is to synthesize these 5 single-site polymers with their specified properties using a metallocene catalyst.

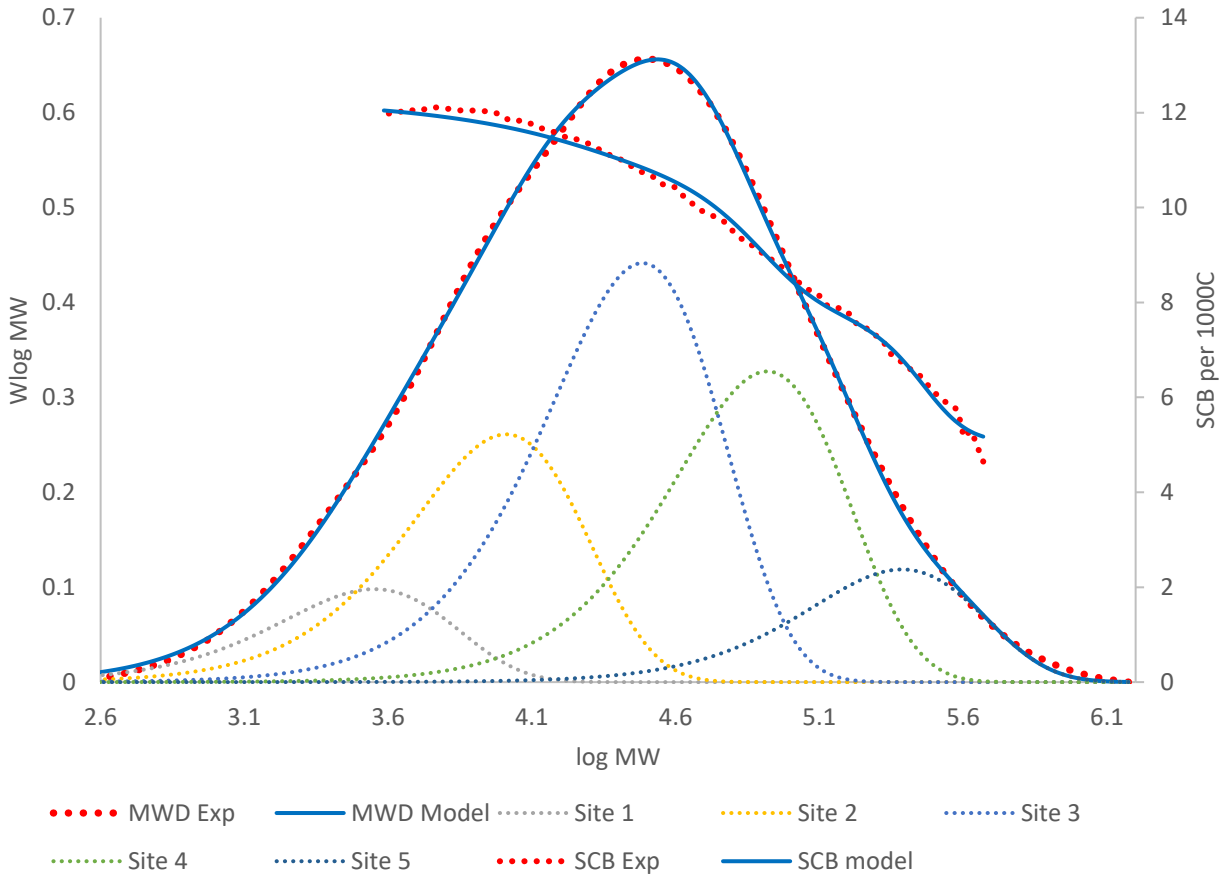

Figure 4-3 MWD and SCBD deconvolution of the ZN polymer. Model parameters are reported in Table 4-2.

Table 4-2 MWD × IR deconvolution parameters for the ZN Polymer.

Sites	1	2	3	4	5
m	0.08	0.21	0.35	0.26	0.10
M_n	1,783	5,125	15,263	41,463	122,030
$\overline{\mathbf{SCB}}$	12.41	12.41	11.51	8.08	5.06
$\overline{F}_B$	0.0261	0.0261	0.0241	0.0167	0.0103

4.3.1 Reconstruction of the MWD-SCBD Results

The polymers were prepared using the single site catalysts and procedure described in Chapter 3. Their synthesis conditions are described in Appendices B and C. Their microstructural characteristics, as determined from their GPC-IR analyses, are presented in Table 4-3. The average values (M_n, SCB, and F_B) for the metallocene polymers agree relatively well with the values identified for each population in Table 4-3. Finally, they were blended in the proportions obtained by the MWD deconvolution and their blend was called B1.

Table 4-3 Microstructural characteristics of polymers made using single-site catalysts to mimic the model polymers described in Table 4-2.

Sample ID	H42	H14	CGC-43	H-41	H-34
m	0.08	0.21	0.35	0.26	0.1
M_n	2,200	5,600	15,000	41,000	110,000
$\overline{\mathbf{SCB}}$	16.1	12.8	10.6	8.6	5.0
$\overline{F}_B$	0.034	0.027	0.022	0.018	0.010

The MWD–SCBD of blend B1 and the ZN polymer are compared in Figure 4-4. The distributions for the blend B1 approximate those of the ZN polymer, except for the SCBD values in the low molecular weight region.

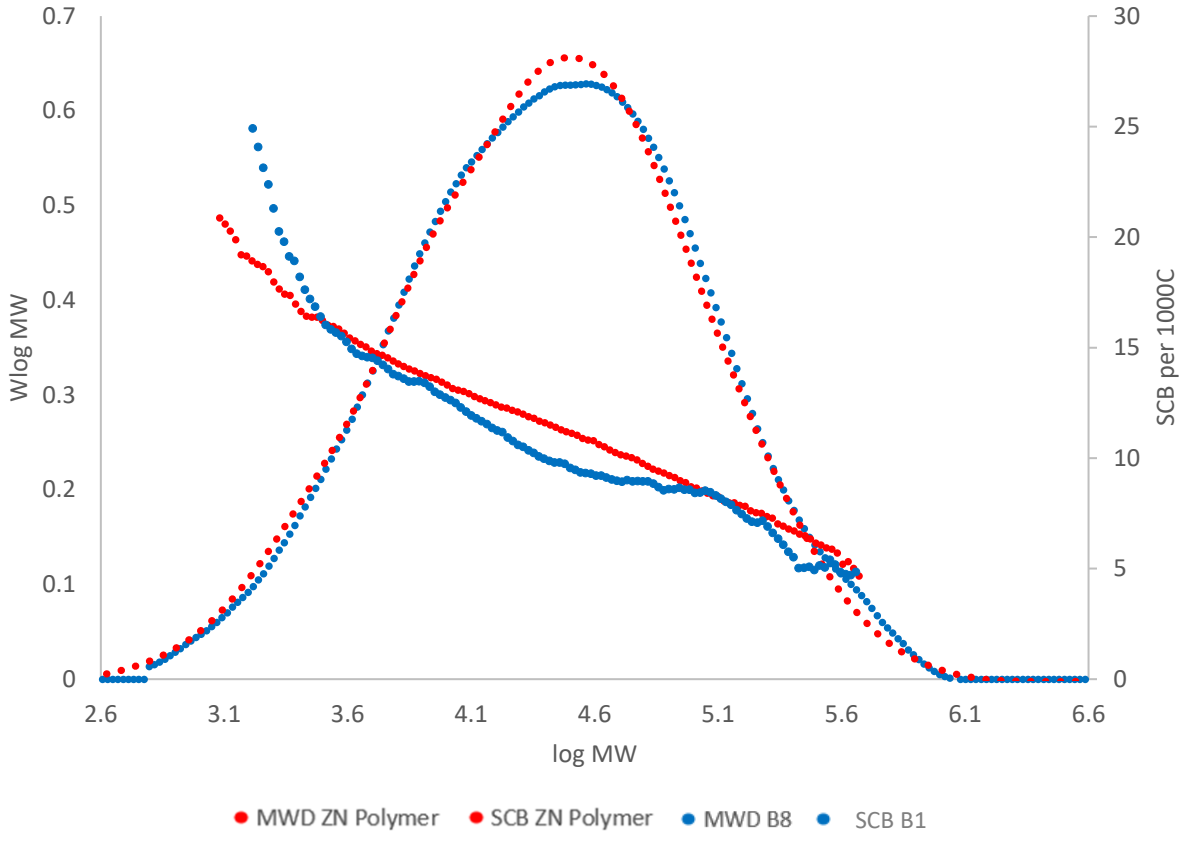

Figure 4-4 MWDs and SCBDs of ZN Polymer and B1.

As a final test, these B1 and the ZN polymer were analyzed by CEF to find out whether their CCDs were as close as their SCBDs (Figure 4-5). Unfortunately, the two CCDs differ substantially. This answers the question: can MWD–SCBD deconvolution eliminate the need for CCD deconvolution? The answer, unfortunately, seems to be no. Since this simpler approach is not enough, in the next sections MWD and CCD deconvolution procedures would be assessed and validated.

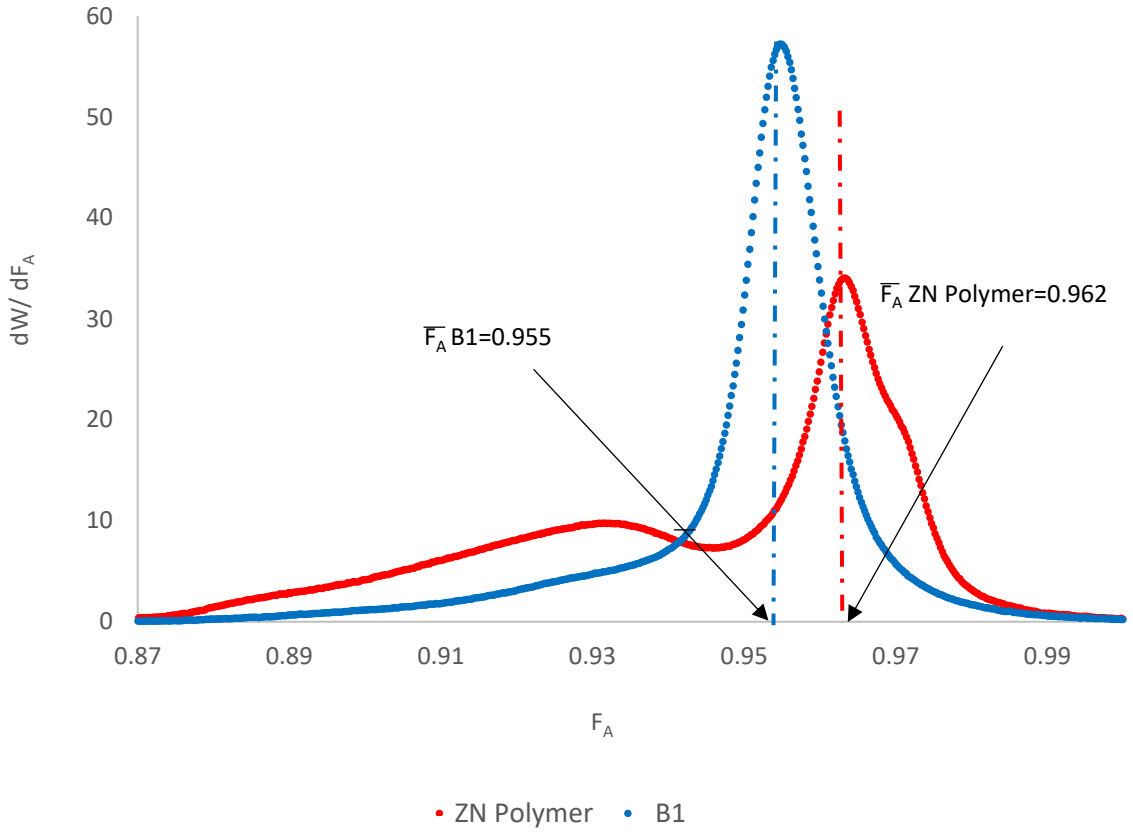

Figure 4-5 CCDs of the experimental blend B1 and ZN polymer.

4.4 MWD and CCD Deconvolution

4.4.1 Deconvolution Approach 1: The Fitting Approach

For all the MWD and CCD deconvolution methods discussed herein, the MWD deconvolution procedure remains the same as described in Section 4.3. The minimum number of Flory distributions required to describe the experimental MWD of the ZN polymer is determined by minimizing the objective function ${\chi_1}^2$ given in Equation (4.2). The parameters m_j, $\hat{\tau}_j$, and the number of site types n were thus were kept the same during all CCD deconvolutions.[44]

The CCD of the ZN polymer was expressed as a sum of the CCDs of polymer made in its individual site types,

$$w\,(F_A) = \sum_{j=1}^{n} m_j \frac{3}{4\sqrt{2\,\beta_j \tau_j}\left[1 + \frac{(F_A - \bar{F}_{Aj})^2}{2\beta_j \tau_j}\right]^{\frac{5}{2}}} \tag{4.6}$$

The values of the parameters β_j and $\overline{F}_{Aj}$ were optimized to describe the experimental CCD distribution of the ZN polymer (measured by CEF) by minimizing the objective function,

$$\chi_3{}^2 = \sum_{i=1}^{n_{CEF}} (w_{F_{A,i}}^{CEF} - w_{F_{A,i}})^2 \tag{4.7}$$

$$\chi_3{}^2 = \sum_{i=1}^{n_{CEF}} \left(w_{F_{A,i}}^{CEF} - \sum_{j=1}^{n} m_j \frac{3}{4\sqrt{2\,\beta_j \tau_j}\left[1 + \frac{\left(F_A - \bar{F}_{Aj}\right)^2}{2\beta_j \tau_j}\right]^{\frac{5}{2}}} \right)^2 \tag{4.8}$$

where n_{CEF} is the number of data points in the CEF distribution, $w_{F_A}^{CEF}$.

It is important to realize that the CEF profile is not CCD, but it is related to it. Consequently, the value of the parameter β obtained through CCD deconvolution is only an apparent value and should not be used to determine the product $r_A r_B$ using Equation (2.2).[3]

The MWD and CCD deconvolution results for 3 site types are shown in Figure 4-6. The value $\chi_1{}^2$ is 0.085 and $\chi_3{}^2$ is 0.169.

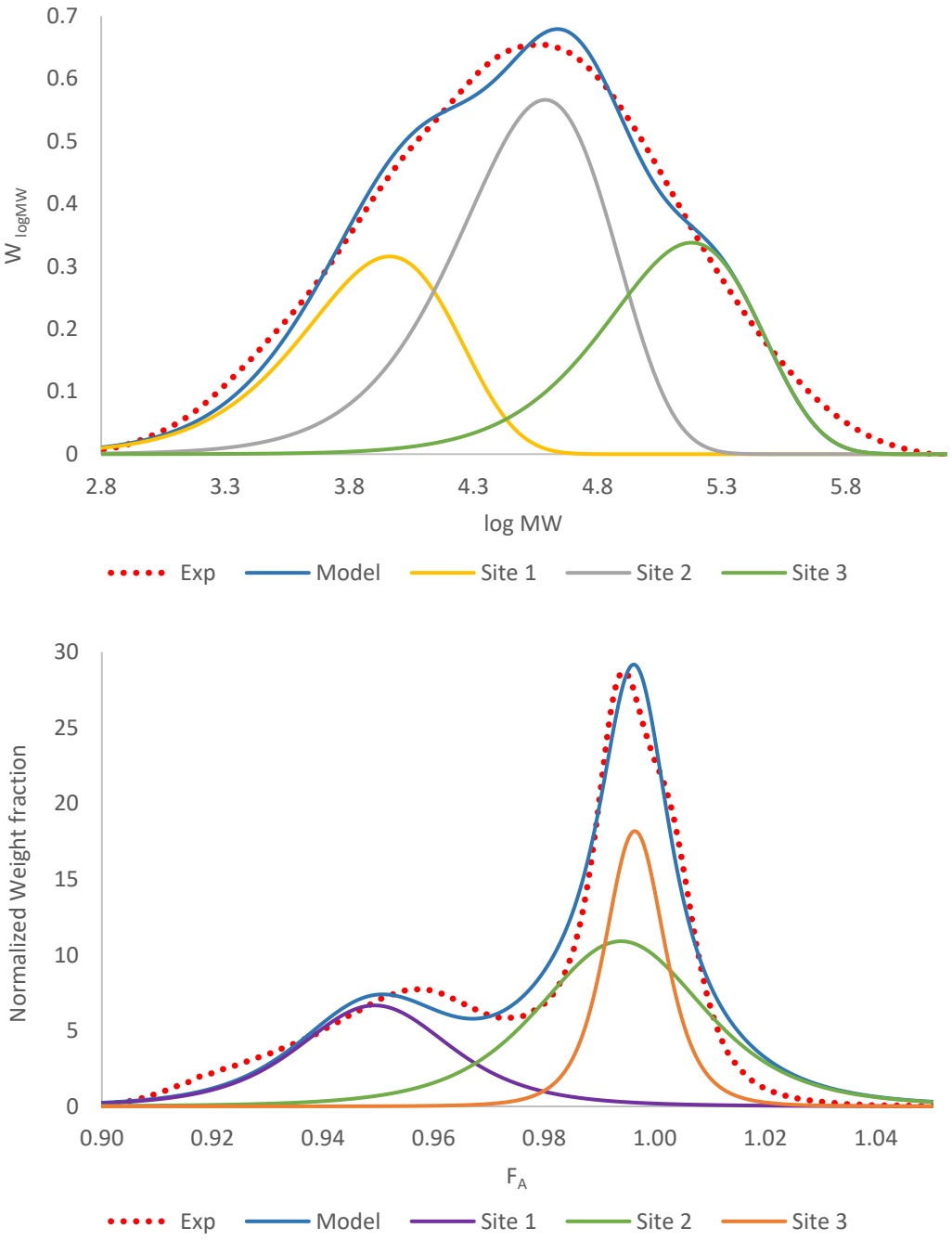

Figure 4-6 MWD and CCD deconvolution results of the ZN polymer using 3 site types. ($\chi_1{}^2$ = 0.085 and $\chi_3{}^2$ = 0.169).

It is evident that the fit could improve by adding another site type. Hence, 4 site types were used, as shown in Figure 4-7 ($\chi_1{}^2$= 0.014 and $\chi_3{}^2$ = 0.0107).

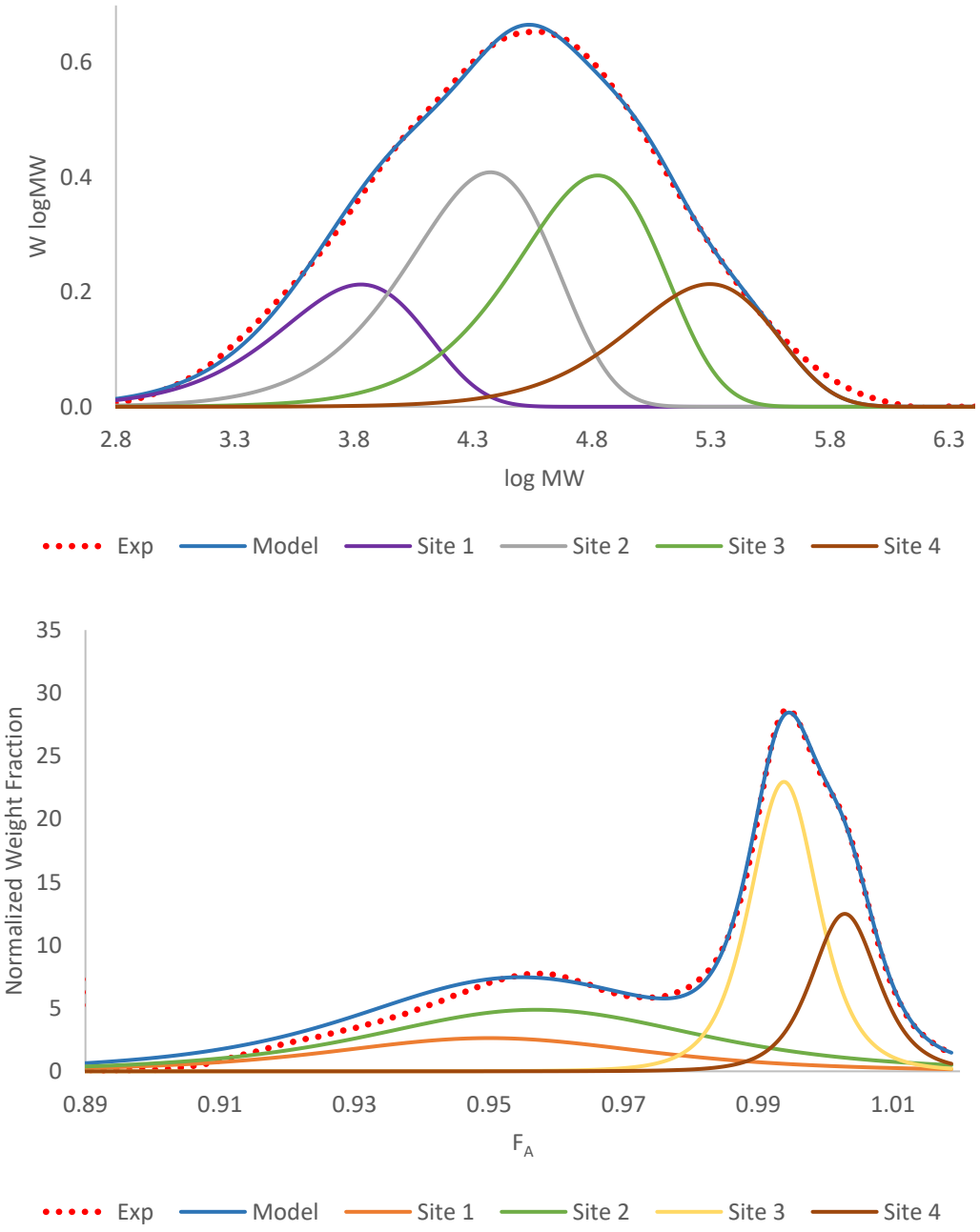

Figure 4-7 MWD and CCD deconvolution results of the ZN polymer using 4 site types. (χ_1^2 = 0.014 and χ_3^2 = 0.0107).

When the number of site types was increased to 5, as shown in Figure 4-8, χ_1^2 dropped even more to 0.002 and χ_3^2 to 0.01. Adding more site types did not lead to a better fit of the MWD or

CCD. Hence, the minimum number of site types required to describe the MWD and CCD of the ZN polymer was found to be 5.

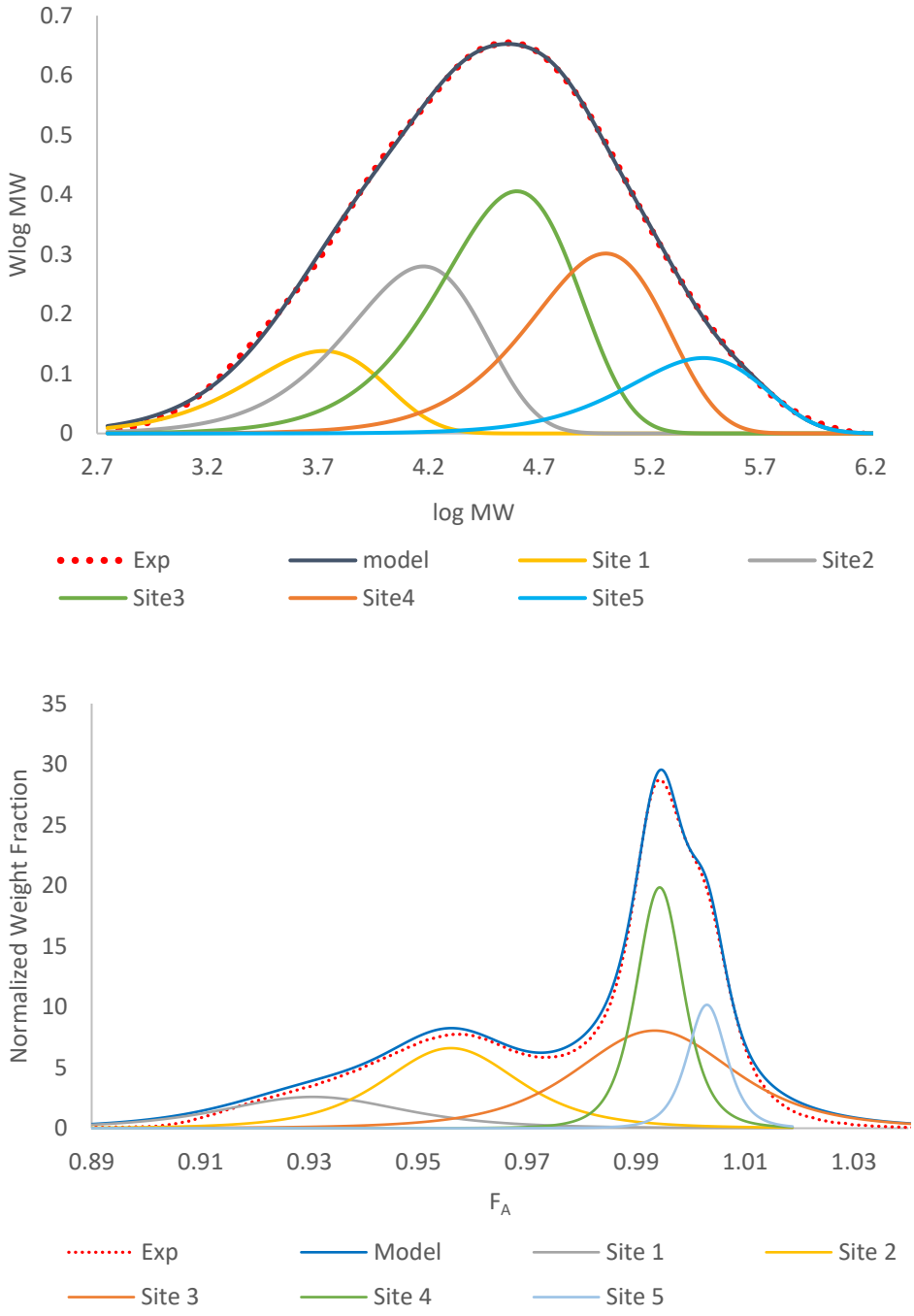

Figure 4-8 MWD and CCD deconvolution results of the ZN polymer using 5 site types. ($\chi_1{}^2 = 0.002$ and $\chi_3{}^2 = 0.010$).

The model parameters estimated from MWD and CCD deconvolution of the ZN Polymer using 5 site types are listed in Table 4-4.

Table 4-4 MWD and CCD deconvolution parameters using 5 site types.

Sites	**1**	**2**	**3**	**4**	**5**
$\boldsymbol{m}$	0.081	0.218	0.354	0.256	0.092
$\boldsymbol{M_n}$	2,106	5,815	16,491	43,618	120,257
$\boldsymbol{\beta}$	0.023	0.059	0.363	0.065	0.104
$\boldsymbol{\bar{F}_A}$	0.927	0.954	0.992	0.995	1.003

Although the model fits the data well, a practical issue arises with the predictions of this approach. The nature of the model polymer targets is unrealistic due to their broadness, thus, making it impossible to synthesize them. The unrealistically broad breadth of the distributions estimated is due to the unrealistic β values. A realistic value of β will show us what polymers can be made. β is defined in Equation (2.4). To calculate a realistic β, the product of $r_A \times r_B$ was taken as 1.16 for the single-site catalyst, Bis(cyclopentadienyl) hafnium (IV) dichloride, used in this thesis from the literature.[46] Then, Stockmayer distributions as given in Equation (2.10) were calculated for each site for *m,* M_n, and $\bar{F}_A$ given in Table 4-4 and the realistic β. The Stockmayer distributions thus calculated were plotted with the CCDs of the model polymer targets and the ZN polymer in Figure 4-9. Comparing their narrow breadths with the model polymers make it clear that the polymers estimated using this approach are impossible to synthesize in reality.

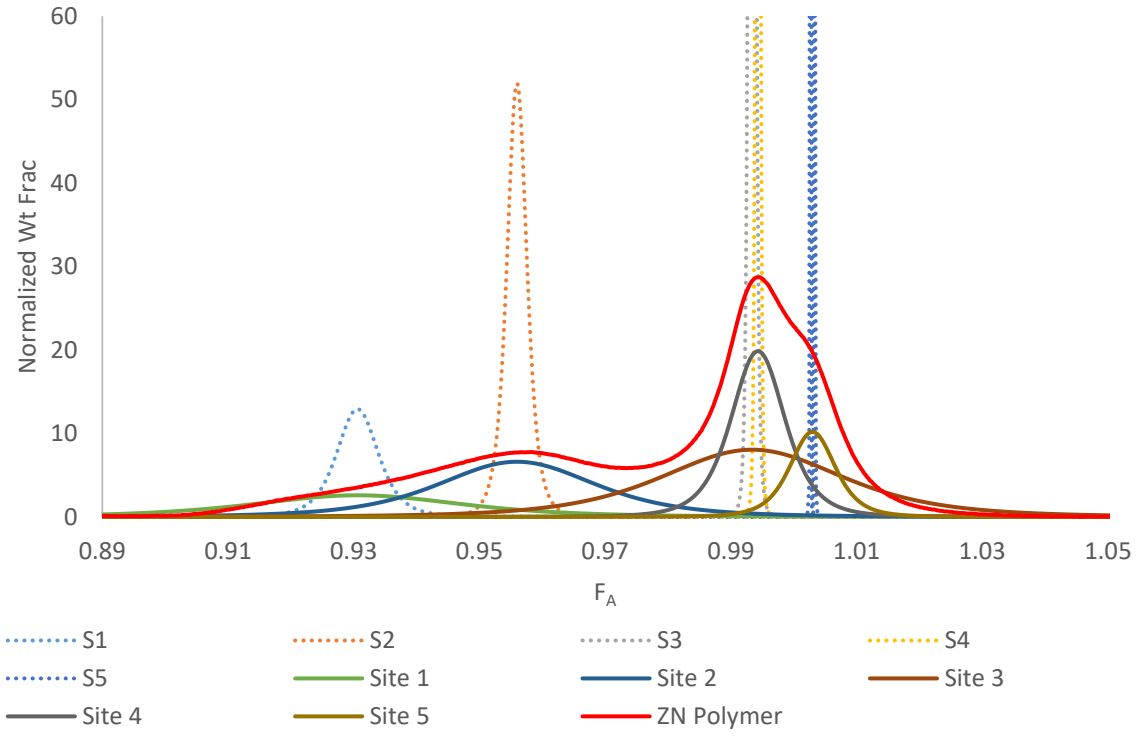

Figure 4-9 CCDs of the model polymers estimated using the Fitting Approach (Site 1-Site 5), the ZN Polymer, and the Stockmayer distributions of the polymers calculated using the realistic β values (S1-S5).

In this approach, β was allowed to vary unconstrained to achieve the best fit ignoring the fact that the CCDs of polymers made using single-site catalysts are not so broad in reality. As a result, the peaks identified are also inaccurate. One way to solve this problem is to constrain β in a way that they are realistic. This is explained in the next section.

4.4.2 Deconvolution Approach 2: the Constrained β Approach

We saw how the model polymer targets predicted by the Fitting Approach were unrealistically broad. In addition, some fundamental issues with b also became apparent. A plot of b x F_A for the single site catalyst for $r_A \times r_B = 1.16$ is shown in Figure 4-10.

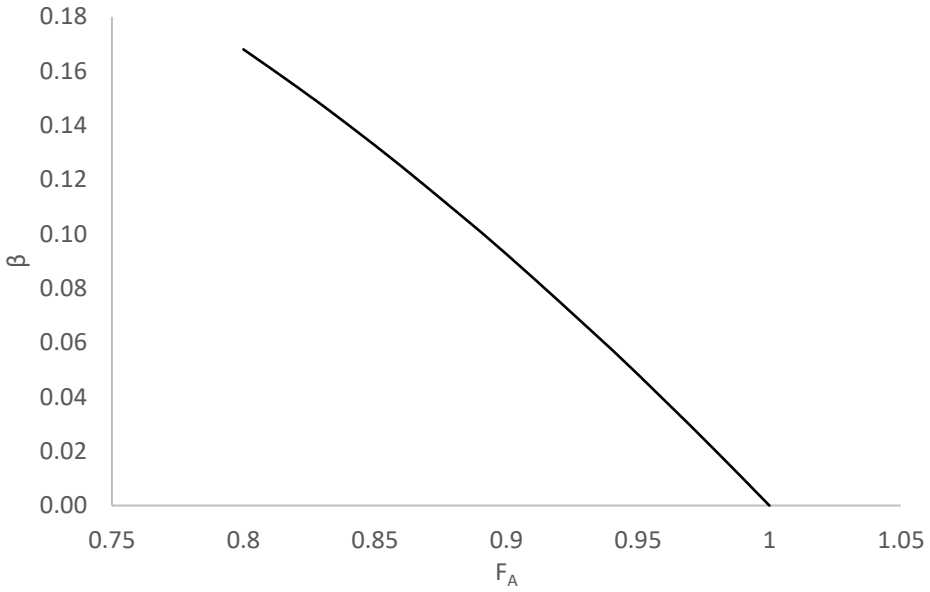

Figure 4-10 Value of the parameter β as a function of $\bar{F}_A$ for $r_A \times r_B$ = 1.16.

The value of β should decrease with an increase in $\bar{F}_A$. However, the values of b found using the Fitting Approach (Table 4-4) do not follow the expected trend. Therefore, β was constrained on $\bar{F}_A$, as discussed in the following section, to make the values more realistic. It should be emphasized again that β is only an apparent value in the model, therefore, it needs not follow the theoretical trend with $\bar{F}_A$. It will only be useful to constrain β if it improves the prediction performance of the model and the aim was to answer if it does improve.

Before the procedure for constraining the β is discussed, it is important to note that the CCDs above were obtained from the CEF temperature profiles using a linear calibration curve, as previously shown in Figure 4-2. To eliminate the effect of calibration curve change over time, I decided to use the raw data (elution temperature) from the CEF analysis. Therefore, the temperature profiles were deconvoluted instead of their corresponding mole fraction profiles. The procedure is described in the following section.

The CEF linear calibration curve is defined as

$$F_A = a + bT \tag{4.9}$$

where, F_A is the ethylene mole fraction of the copolymer and T is the elution temperature.

Correspondingly, for the averages, the calibration curve can be defined as

$$\bar{F}_A = a + bT_p \tag{4.10}$$

where, T_p is the peak elution temperature and $\bar{F}_A$ is the average ethylene mole fraction of the copolymer.

When $\bar{F}_A$ from Equation (4.10) is replaced in Equation (2.4), we get

$$\beta = \left(a + bT_p\right) \times \left[1 - \left(a + bT_p\right)\right] \sqrt{1 - 4 \times \left(a + bT_p\right) \times \left[1 - \left(a + bT_p\right)\right] \times (1 - r_A \times r_B)} \tag{4.11}$$

Thus, β is dependent on T_p. In this approach, β was not an independent variable and was not allowed to change to reach optimization. Instead, it was constrained on T_p using realistic r_A, r_B values. The product $r_A \times r_B$ was kept as 1.16 which is true for the catalyst used and is also representative of most single-site catalysts.[46,47] T_{pj} were estimated by minimizing the objective function defined in Equation (4.12).

When F_A from Equation (4.9) and $\bar{F}_A$ from Equation (4.10) are replaced in Equation (4.8) we get

$$\chi_4{}^2 = \sum_{i=1}^{n_{CEF}} \left(w_{F_{A,i}}^{CEF} - \sum_{j=1}^{n} m_j \frac{3}{4\sqrt{2\,\beta_j \tau_j}\left[1 + \frac{b\left(T - T_{pj}\right)^2}{2\beta_j \tau_j}\right]^{\frac{5}{2}}} \right)^2 \tag{4.12}$$

Note that the changes in the approach were only on the CCD deconvolution part, the MWD deconvolution procedure, and hence, its results remained the same.

Figure 4-11 shows the CCD deconvolution results for the ZN polymer using the constrained β approach. Table 4-5 shows the values estimated for the parameters.

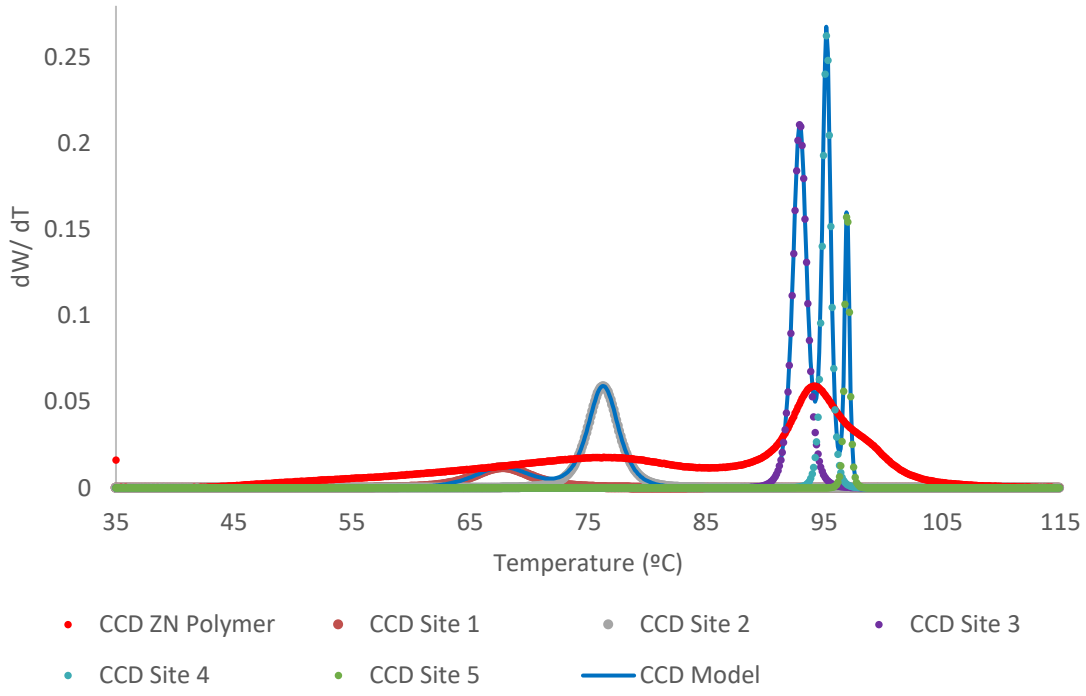

Figure 4-11 CCD deconvolution of ZN Polymer using the Constrained β approach.

Table 4-5 MWD and CCD deconvolution parameters by the Constrained β approach for the ZN Polymer.

Sites	1	2	3	4	5
m	0.081	0.218	0.354	0.256	0.092
M_n	2,106	5,815	16,491	43,618	120,257
β	0.077	0.064	0.037	0.033	0.030
T_p	67.75	76.27	92.94	95.20	96.93

The key features of this approach are

- the lower degrees of freedom (10→5), presumably leading to better peak identification

- realistic values of β, thus better chances of synthesizing the target model polymers identified by deconvolution.

4.4.2.1 Results of Deconvolution Approach 2: The Constrained β Approach

Two different sets of copolymers were available that mimicked the model polymers predicted using the Constrained β Approach. Table 4-6 and Table 4-7 summarizes the microstructural properties of these copolymers. Their synthesis conditions are described in Appendices B and C. The polymers were blended to create two different blends: B2 and B3.

Table 4-6 Microstructural characteristics of the polymers synthesized to mimic the model polymers described in Table 4-5 (Constrained β Approach) and blended to form the blend B2.

Site	**1**	**2**	**3**	**4**	**5**
Sample ID	H-20	H-59	H-52	H-77	H-82
M_n	2,800	4,500	16,000	41,000	100,000
M_w	4,900	10,500	36,000	100,000	260,000
T_p	68.4	79.8	90.1	95.2	93.5

Table 4-7 Microstructural characteristics of the polymers synthesized to mimic the model polymers described in Table 4-5 (Constrained β Approach) and blended to form the blend B3.

Site	**1**	**2**	**3**	**4**	**5**
Sample ID	H-44	H-63	H-56	H-79	H-82
M_n	1,800	4,800	13,000	49,000	100,000
M_w	3,500	11,000	30,000	100,000	260,000
T_p	71.9	81.6	90.3	94.9	93.5

The two blends and the ZN polymers were characterized for their MWDs (Figure 4-12) and CCDs (Figure 4-13). The MWDs of the blends agree with that for the ZN polymer. The CCDs, on the other hand, differ. The high and low-temperature peaks of the CCD of the ZN polymer and the blends coincide, but the areas under them do not.

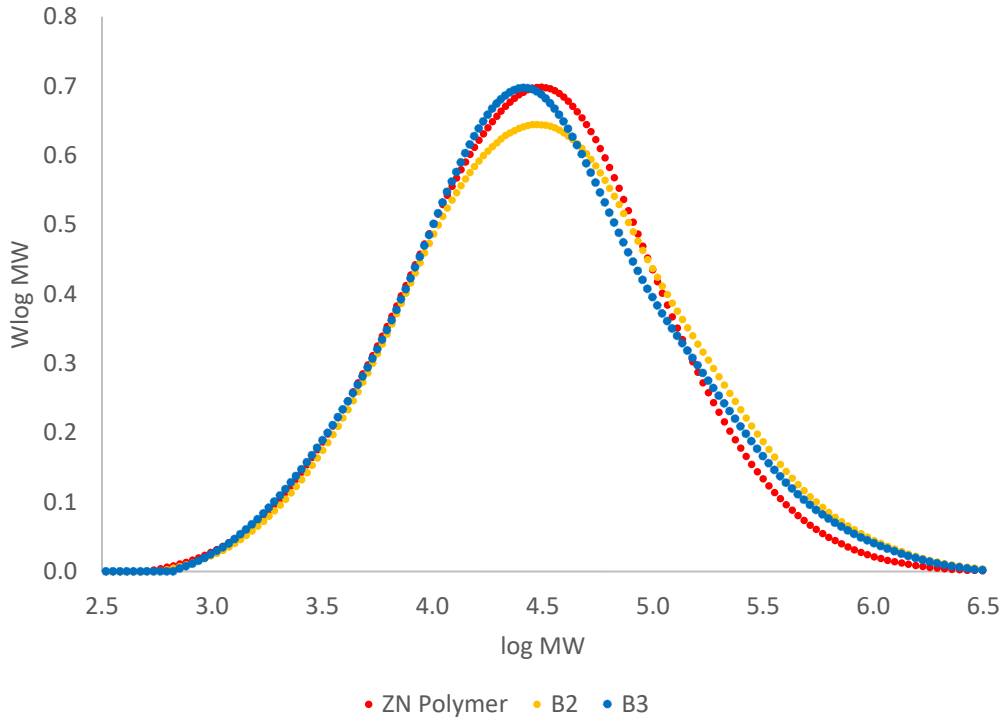

Figure 4-12 MWD of the ZN Polymer, Blend B2, and Blend B3.

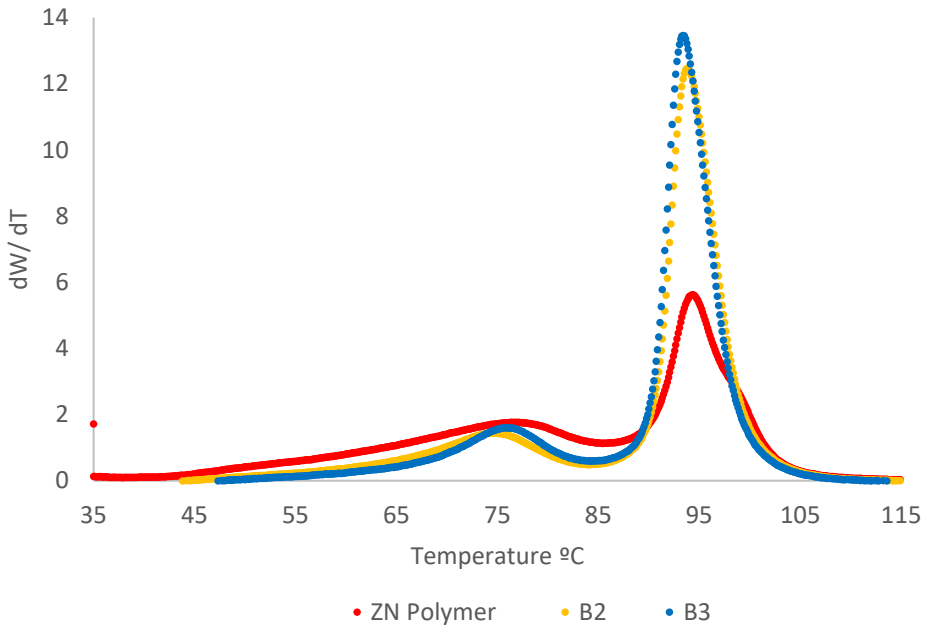

Figure 4-13 CEF Profiles of ZN Polymer, Blend B2, and Blend B3.

The DSC profiles of the ZN Polymer and Blend B3 are compared in Figure 4-14. The crystallization and melting peaks are similar, but the overall melting and crystallization profiles differ, which agrees with the CEF results depicted in Figure 4-13.

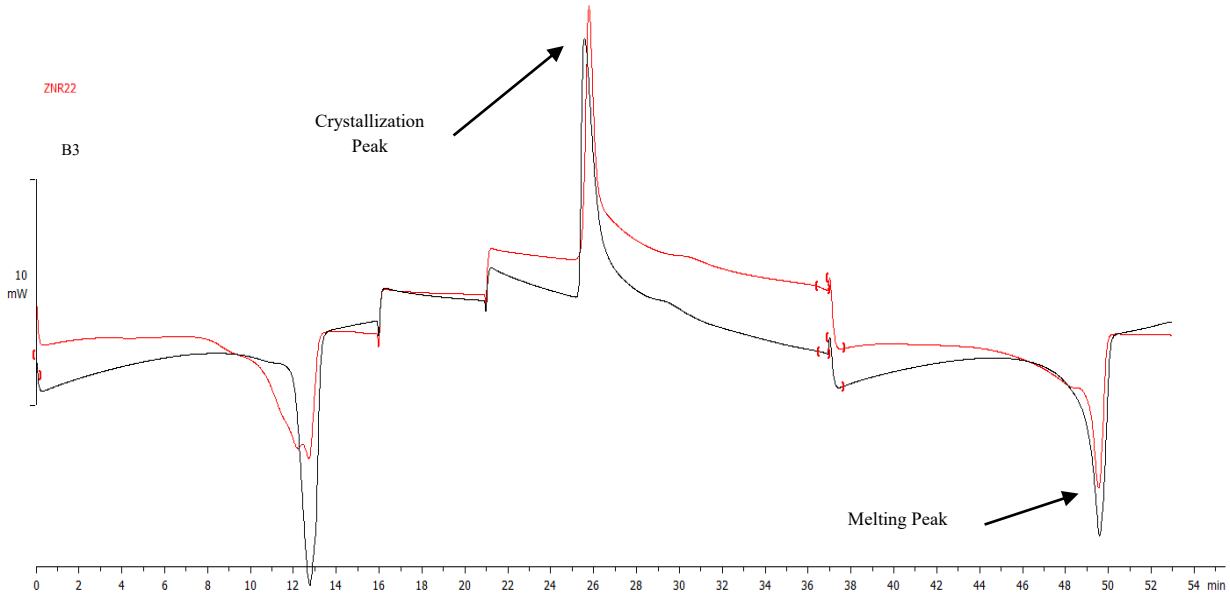

Figure 4-14 DSC Profiles of ZN Polymer, and Blend B3.

4.4.3 Deconvolution Approach 3: The Boundary Conditions Approach

Figure 4-13 shows that the areas under the high and low-temperature peaks of the blend CCD are different from those for the ZN polymer. When the modeling and experimental results of the Constrained β Approach are compared in Figure 4-15, the picture becomes clearer. The experimental results for the blend agree with the model targets, but they do not represent the CCD of the ZN Polymer. This mismatch may be caused for two main reasons:

1. The area under the sites (proportional to the mass of polymer made on each site type, m) is incorrectly determined by the model. The mass of polymer made on site types 1 or 2 need to be larger, and the mass of polymer made on site types 3 to 5 need to be lower for a better fit of the ZN Polymer.

2. The peak temperature identified for at least some of the site types is incorrect. For example, the peak temperature for Site 3 may be lower than the one shown in Figure 4.15.

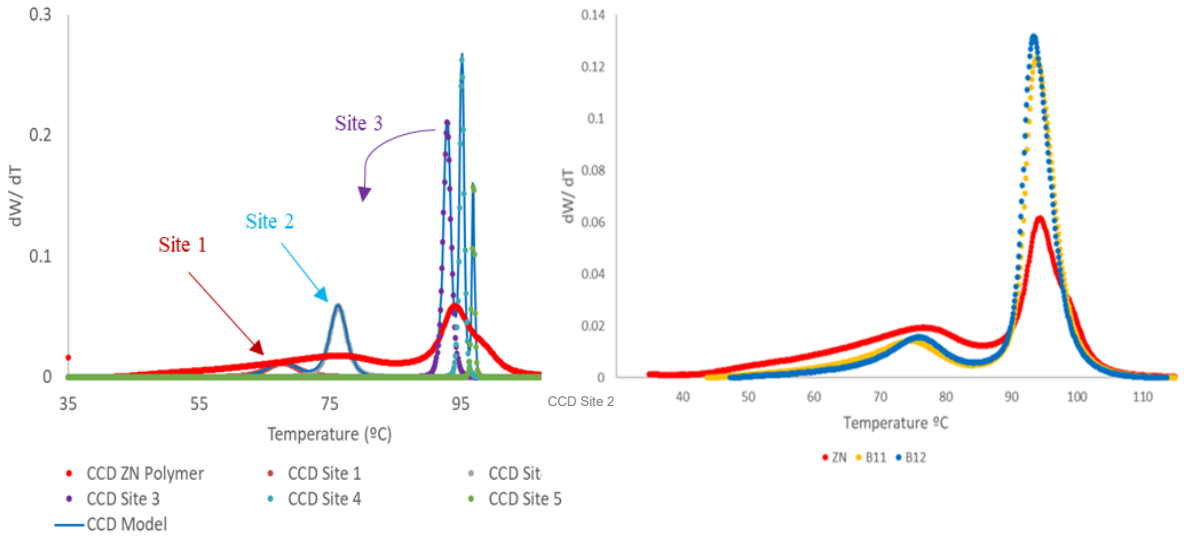

Figure 4-15 Modeling (left) and the experimental (right) results of the Constrained β Approach.

The mass fraction of polymer produced on each site type, m, is determined by MWD deconvolution. In contrast to the CCD deconvolution procedure, there are no apparent parameters — such as β — in the MWD deconvolution method. Therefore, the parameters m and M_n can be considered more reliable, as proven by the good representation of the MWD of the ZN Polymer (Figure 4-12). Consequently, the areas of the individual sites in the CCD deconvolution procedure are likely to be accurate, which rules out explanation 1 above. This brings us to the next potential cause for the CCD mismatch: the incorrect position of the sites.

Table 4-8 uses the values identified for the parameter m in Table 4-5 to calculate the cumulative mass percentages, m_c %, for the blend. These cumulative mass percentages can be used to help identify the correct peak temperatures for the model polymers.

Table 4-8 Maximum threshold temperatures for each site type.

Sites	**1**	**2**	**3**	**4**	**5**
$\boldsymbol{m}$	0.081	0.218	0.354	0.256	0.092
$\boldsymbol{m_{c\%}}$	8.1	29.9	65.2	90.8	100
$\boldsymbol{T_c}$ (°C)	35	72.3	92.9	98.3	135

The differential and cumulative CEF curves for the ZN polymer are compared in Figure 4-16. The CEF profile can be subdivided into temperature intervals, T_c, that correspond to the $m_{c\%}$ values in Table 4-8 by comparing the cumulative CEF curve with the $m_{c\%}$ values, as shown in Figure 4-17. Therefore, the correct peak temperature of the polymer populations made in site type 1 ($m_{c\%}$ = 8.1%) correspond to $T_{p1} \leq 35$ °C, in site type 2 to 35 °C < $T_{p2} \leq 72.3$ °C, and so on. This way in this approach, T_{pj} were bounded within the identified temperature intervals to which the polymer populations must belong to more closely match the areas of the CEF curve for the ZN Polymer. With this added constraint, T_{pj} were estimated by minimizing the objective function defined in Equation (4.12).

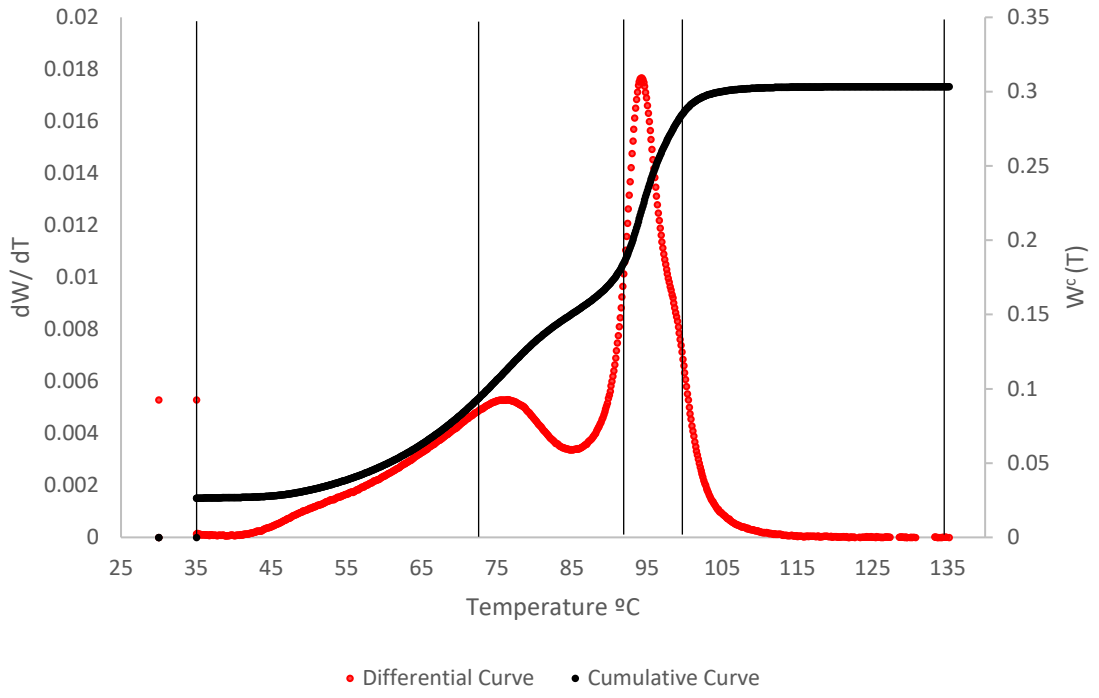

Figure 4-16 The cumulative and differential CEF profile of the ZN Polymer with the defined temperature boundary conditions.

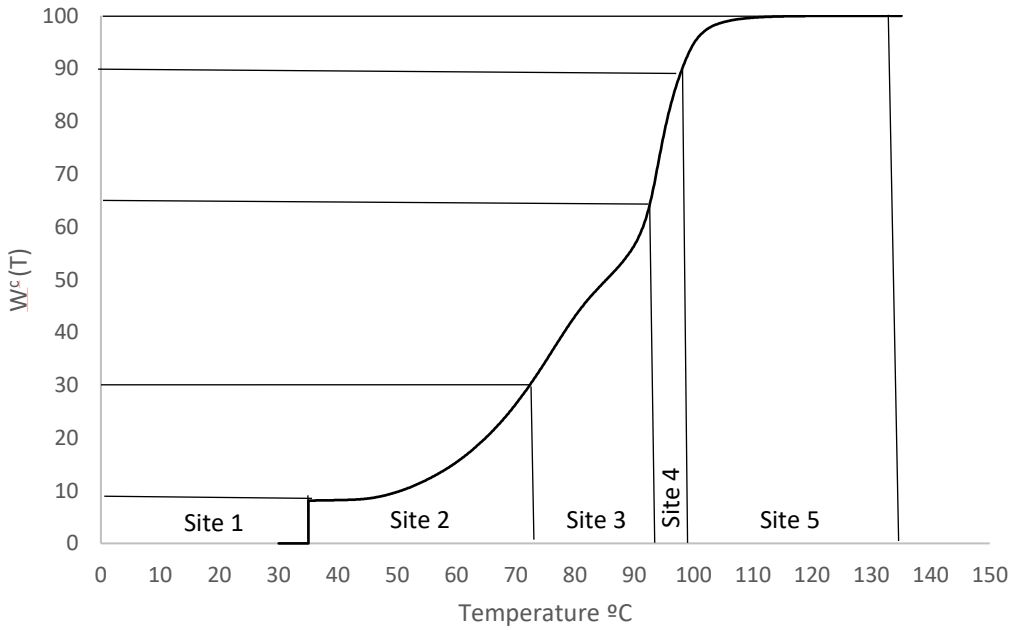

Figure 4-17 The cumulative CEF curve for the ZN polymer.

Figure 4-18 shows where the populations identified with the Constrained β Approach (Table 4-5) are located in the cumulative and differential CEF profiles of the ZN Polymer. Comparing these locations with those in Figure 4-17, it is easy (in retrospect) to conclude that would never agree with the cumulative CEF profile.

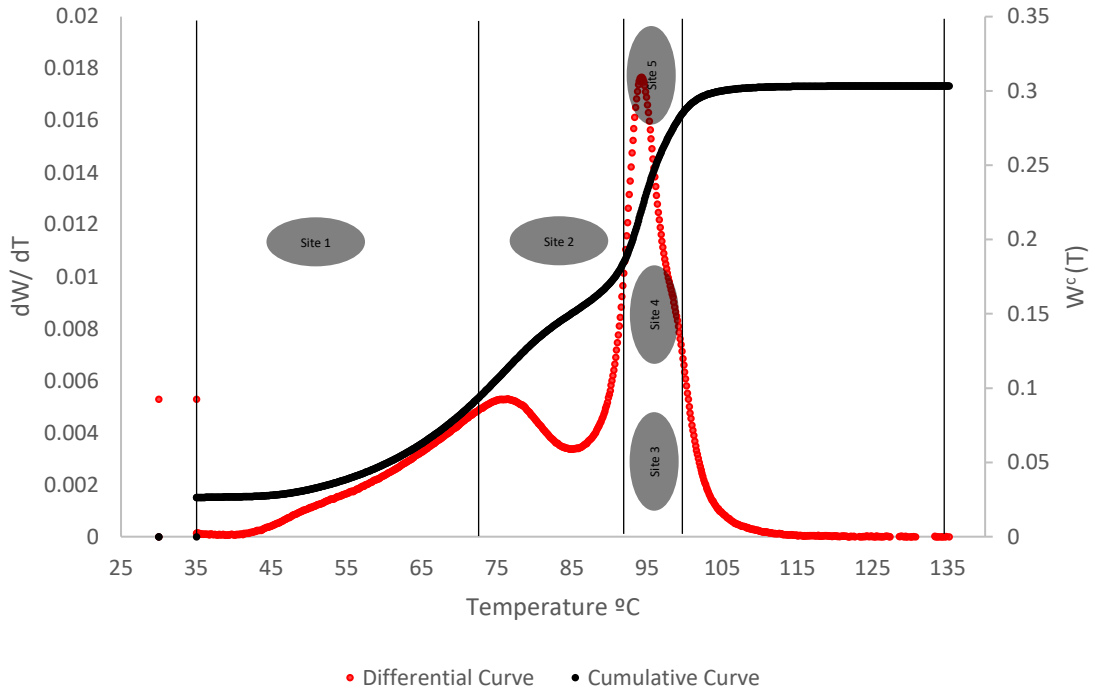

Figure 4-18 Peak positions for populations identified with the Constrained β Approach on the cumulative and differential CEF profiles of the ZN Polymer.

In the Boundary Conditions Approach, constraints were imposed on the peak elution temperature T_{pj} for each population to make sure they fell within the adequate temperature range. The deconvolution results with this new method are shown in Figure 4-19 and the parameters are listed in Table 4-9.

The key features of this improved approach are:

1. The mass balance for the cumulative CEF profile is obeyed.
2. The polymer populations are more evenly distributed.

Finally, even though the model does not fit with the experimental CEF curve of the ZN Polymer well because the individual peaks are too narrow, co-crystallization effects during the CEF fractionation of the blend are expected to broaden its experimental profile.

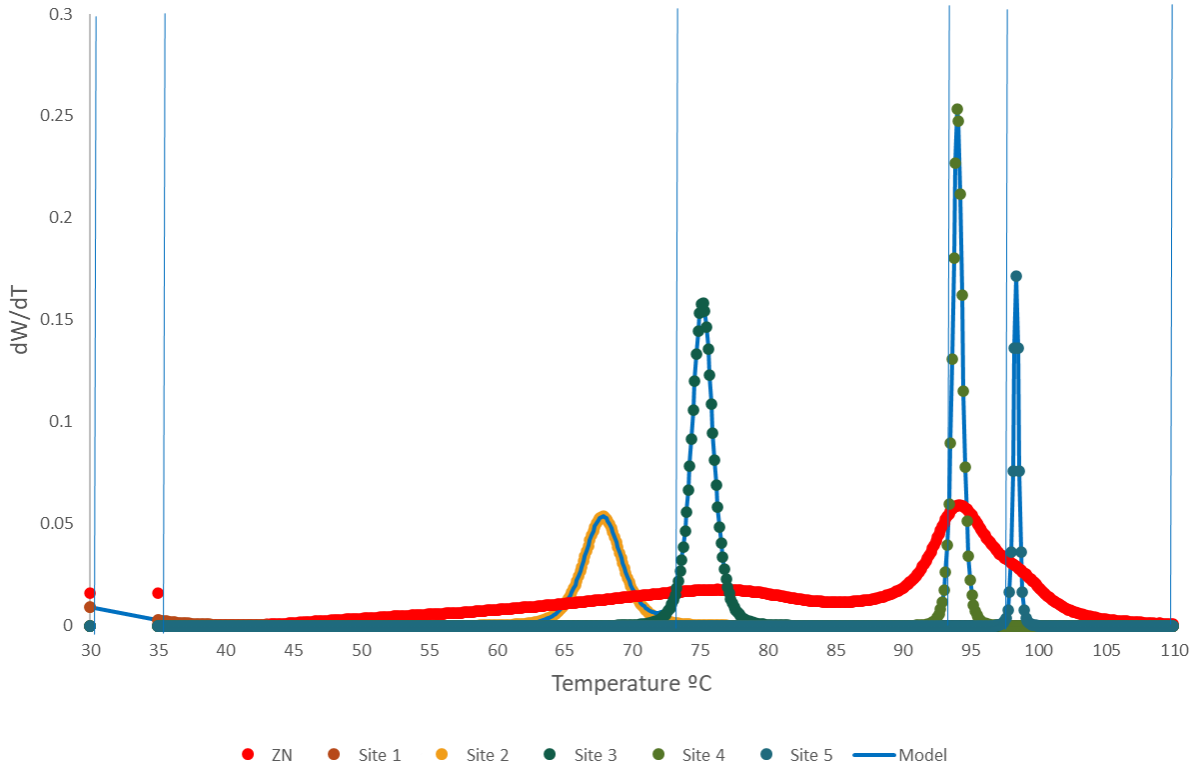

Figure 4-19 CCD deconvolution of ZN using the Boundary Conditions Approach.

Table 4-9 Parameters estimated for CCD deconvolution of ZN using the Boundary Conditions Approach.

Sites	1	2	3	4	5
m	0.081	0.218	0.354	0.256	0.092
β	0.13	0.08	0.07	0.03	0.03
T_p	30	67.83	75.18	94.01	98.33

4.4.3.1 Results of Deconvolution Approach 3: The Boundary Conditions Approach

The model polymers, predicted by the Boundary Conditions Approach, were synthesized and their microstructural properties are detailed in Table 4-10. Their synthesis conditions are described in Appendices B and C. These model polymers were blended to form Blend B4.

Table 4-10 Microstructural characteristics of the polymers synthesized to mimic the model polymers described in Table 4-10 (the Boundary Conditions Approach) and blended to form the blend B4

Site	**1**	**2**	**3**	**4**	**5**
Sample ID	CGC 52	H 62	C53	H 77	CGK 26
M_n	2,400	4,300	17,000	41,000	130,000
M_w	4,400	9,600	40,000	100,000	260,000
T_p	30.00	70.6	75.4	95.2	97.00

The CEF profiles for Blend B4 and the ZN Polymer are compared in Figure 4-20. Even though the blend profile matches the ZN Polymer profile much better than in the previous method (Figure 4-14), the peak positions are still shifted, particularly the low-temperature peak.

The CEF profile for the blend formed two main peaks: one below 75 °C and the other above 95 °C. In contrast, the CEF profile for the ZN Polymer is more evenly spread, with a substantial fraction of polymer between 75 and 95 ºC. Table 4-10 shows a significant temperature difference (approximately 20 °C) between the peak temperatures of populations made on Site 3 and 4, but small temperature differences (approximately 5 °C) between polymers made on Site 2 and 3, and 4 and 5. Even at the slow cooling rates using in the CEF analysis, polyolefins tend to co-crystallize when their peak temperatures are close.[48] Therefore, it seems likely that the polymers made to represent the populations in Site 2 and 3, and Site 4 and 5 co-crystallized during CEF analysis, creating the valley observed in the 75 - 95 °C range.

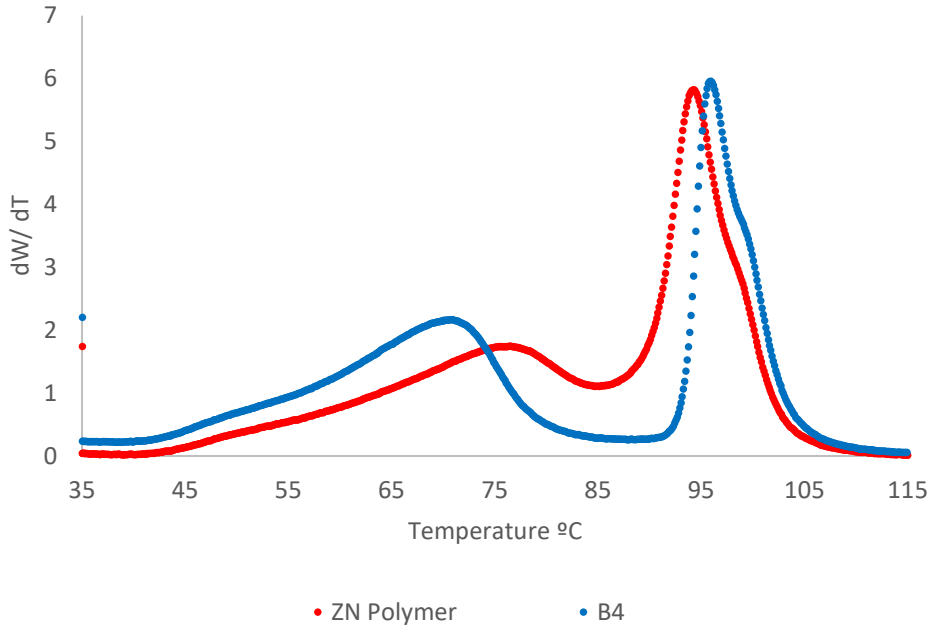

Figure 4-20 CEF Profiles of the ZN Polymer and blend B4.

When we see the estimated peak temperatures for the polymers made on sites 2 and 3 in Figure 4-21, it is apparent that the optimization process chose the model peak positions near the high and low peaks of the ZN polymer curve to minimize the error. As a result, these peak positions are not often centered in their respective bounded temperature range but could be very close to the boundaries as illustrated in Figure 4-21. The actual polymer profiles are not strictly as narrow as the theoretical distributions described here. As these peaks are estimated so close to the threshold temperature boundary, due to their broad distributions there is still the chance of mass balance violation. In the next approach, measures were taken to avoid this potential risk and to see how it manifests in the experimental results.

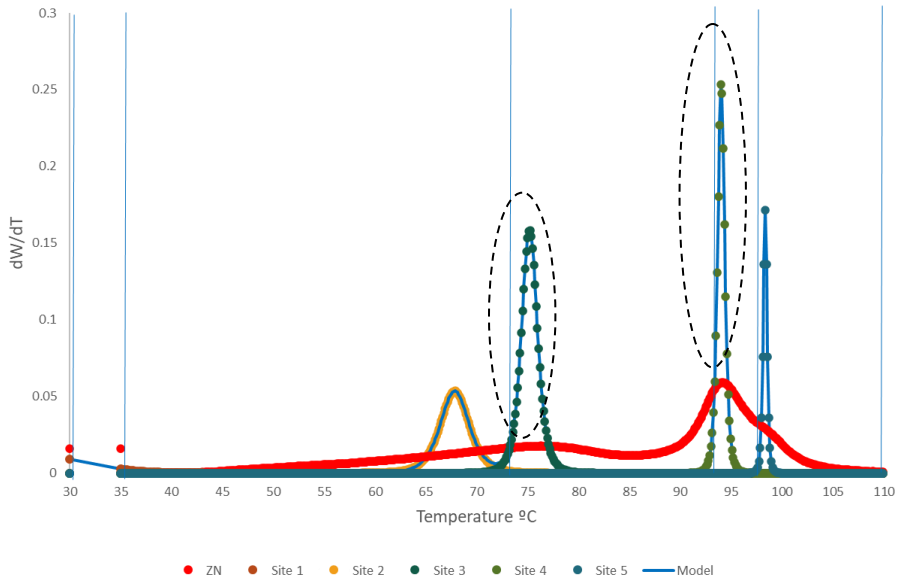

Figure 4-21 CCD deconvolution of ZN using the Boundary Conditions Approach depicting sites close to the temperature boundaries.

DSC analyses were also performed on the ZN Polymer and Blend B4 (Figure 4-22). The crystallization peaks and the melting peaks are close, but the profiles differ.

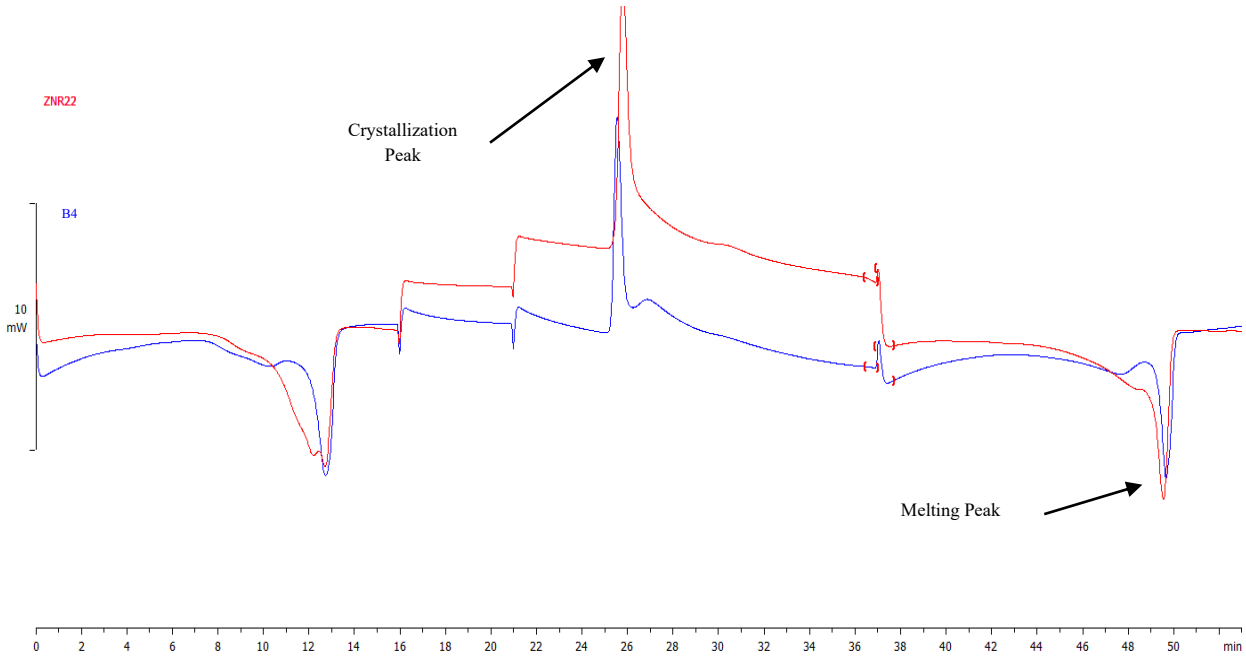

Figure 4-22 DSC Profiles of the ZN Polymer and Blend B4.

4.4.4 Deconvolution Approach 4: The Pragmatic Approach

All optimization methods attempted before (unconstrained and constrained) failed to replicate the CEF profile of the ZN Polymer correctly, probably because none of them accounted for the complex co-crystallization effects taking place during CEF fractionation. The Pragmatic Approach does not attempt to find the peak temperature positions of the polymer populations by any optimization method. Instead, for each site type, the median temperatures T_m that corresponds to the temperature interval that agree with the mass fraction identified by MWD deconvolution for each site type were calculated and assumed to be the target peak temperatures of the polymers made on the sites. The parameters thus determined are listed in Table 4-11. Stockmayer distributions for the individual sites and the overall model were then calculated and plotted along with the distribution of the ZN Polymer, as shown in Figure 4-23. Since the Stockmayer distributions were calculated on the basis of the median temperature, the distributions of each model site were now centered in their respective temperature interval. The fit of this model was also poor, but at least the mass fractions of polymer in each temperature interval for the ZN Polymer and the metallocene polymers agreed.

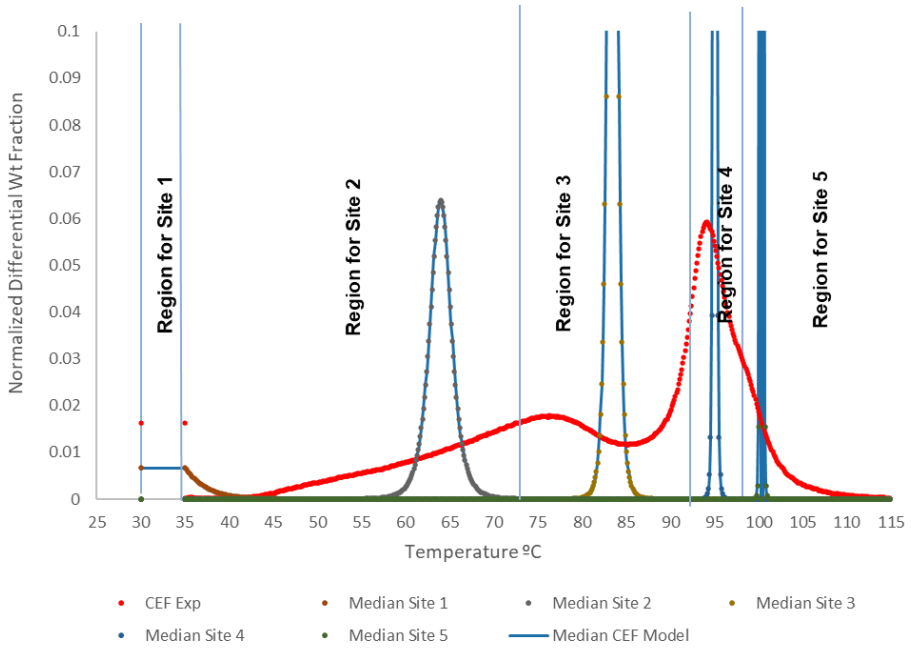

Figure 4-23 CCD deconvolution of the ZN Polymer using the Pragmatic Approach.

Table 4-11 Parameters estimated for CCD deconvolution of the ZN polymer using the Pragmatic Approach.

Sites	1	2	3	4	5
m	0.081	0.218	0.354	0.256	0.092
β	0.101	0.054	0.023	0.004	-0.005
T_m	32.5	63.98	83.45	95.06	100.39

Polymers were made to mimic the target model polymers determined using the Pragmatic Approach. Their properties are summarized in Table 4-12. Their synthesis conditions are described in Appendices B and C. These polymers were blended to form Blend B5.

Table 4-12 Properties of polymers synthesized to represent the model polymers described in Table 4-12 (the Pragmatic Approach) and blended to form the blend B5.

Site	1	2	3	4	5
Sample ID	CGC-52	A2	CGC-30	Hf-77	CGK-26
M_n	2,400	6,600	15,000	41,000	130,000
M_w	4,400	13,000	37,000	100,000	260,000
T_p	30	60.8	84	95.2	98

The MWDs for Blend B5 and the ZN Polymer are compared in Figure 4-24, and they are quite close.

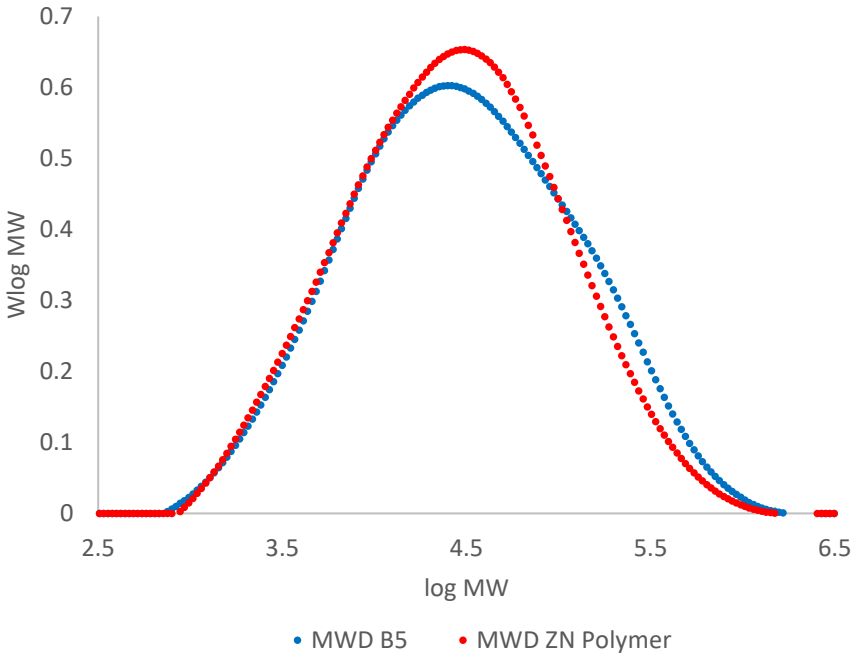

Figure 4-24 MWDs of the ZN Polymer and Blend B5.

The CEF profiles for Blend B5 and the ZN Polymer are compared in Figure 4-25. Even though it is far from perfect, this was the best match found among all methods compared in this thesis. A slight mismatch around the major peak of the ZN Polymer, around 95 °C, may be due to the unavailability of the exact polymer for the polymers made on site 4. The M_W needed was 88,000 but one with 100,000 was synthesized and used in the blend. This might have pushed the overall distribution towards the right resulting in the slight mismatch even though the peak temperature for the polymers made on this site is very close to the targeted peak temperature.

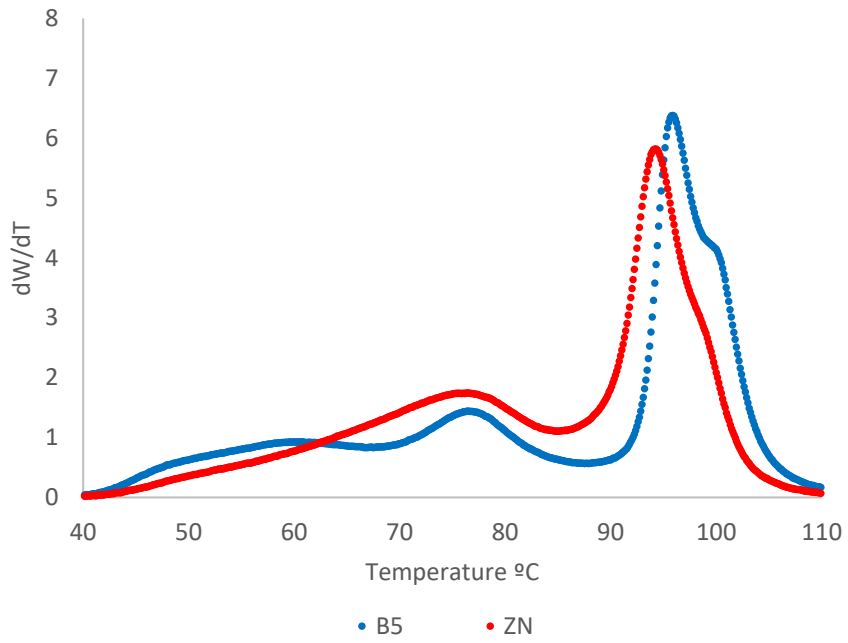

Figure 4-25 CEF profiles of the ZN Polymer and Blend B5.

DSC analyses performed on the ZN Polymer and Blend B5 are shown in Figure 4-26. The crystallization peaks, the melting peaks, and the overall profiles are closer to each other than any other blend made in this investigation.

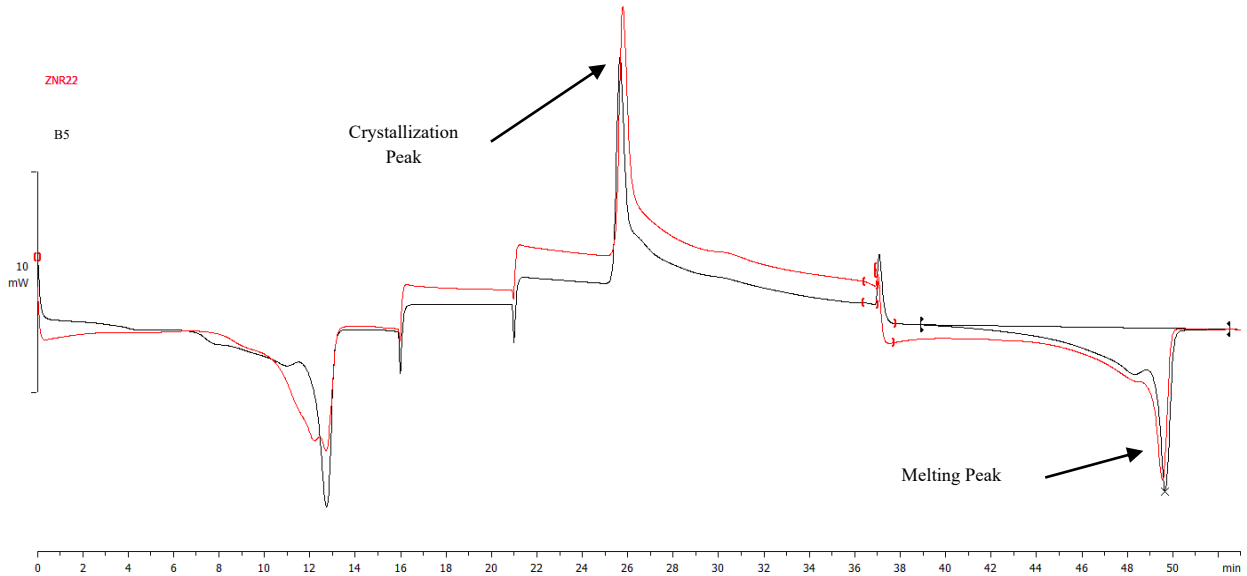

Figure 4-26 DSC profiles of the ZN Polymer and Blend B5.

Chapter 5
Conclusions and Future Work

In this thesis, we set out to validate the prevalent MWD and CCD deconvolution procedures experimentally. MWD deconvolution procedure was easier to validate. The parameters given by the MWD deconvolution are reliable; on the contrary, because of apparent parameter like β, the parameters obtained from the CCD deconvolution are not, and therefore, multiple solutions are possible. Also, the CCD deconvolution procedures do not account for the complex co-crystallization effects taking place during CEF fractionation.

Polymers made using single-site catalysts based on the determined MWD deconvolution parameters were blended and the MWD distribution of the blend matched the parent MWD of the polymer made using the Zeigler-Natta catalyst.

SCBD is an average of the CCD and is determined along with MWD in a single analysis in the GPC-IR. Therefore, the idea was to check if similar SCBD of the blend and the polymer made using the Zeigler-Natta catalyst also ensured their CCDs to be alike. The results showed that that is not the case. Similar SCBDs do not ensure similar CCDs, hence, additional analysis to measure the CCD and its modeling is important to completely understand the nature of the microstructure of a polyethylene sample.

Subsequently, 4 approaches of CCD deconvolution were developed, and their predictive powers were compared. It was found that the prevalent CCD deconvolution approach was rather naïve; it predicted polymers that were impossible to make, paving the way to improve the approach to make more realistic predictions. In the 2nd approach, polymerization fundamentals were used to constrain the β parameter to ensure realistic predictions. The prediction improved as a result, but there was scope for improvement. Investigating further, it turned out that the more fundamental mass balance conservation was not being respected in the previous methods; setting up boundary conditions on the peak temperature targets to ensure the same was the basis of the development of the 3rd approach. The prediction power improved significantly, but there was still a slight mismatch. As it turned out, the boundary conditions applied were not enough to ensure the mass balance and possible co-crystallization further exacerbated the inaccuracy in the predictions.

Finally, in the 4th approach, for each site type, the median temperatures T_m that corresponds to the temperature interval that agrees with the mass fraction identified by MWD deconvolution for each site type were calculated and assumed to be the target peak temperatures of the polymers made on the sites. Hence, the mass balance violation was avoided to the maximum extent. The characterization results from GPC, CEF, and DSC analyses showed that this rather simple method has the best prediction power of them all.

In conclusion, both MWD and CCD of the polymer made using the Zeigler-Natta catalyst were reproduced to a fair extent using a blend of polymers made using the single-site metallocene catalysts. The next step should be to try reproducing the MWD and CCD of more polymers made using different Zeigler-Natta catalysts by applying the successful deconvolution method developed in this thesis to check their universality.

With MWD and CCD of the ZN polymer and blend appearing the same, their mechanical properties should be tested. This is to check if the similarity in their microstructural distributions translates to similarities in their mechanical properties as well. If successful, it would further increase the application of these deconvolution approaches.

References

1. Plastics – the Facts 2018. Accessed June 4, 2021. https://www.plasticseurope.org/application/files/6315/4510/9658/Plastics_the_facts_2018_AF_web.pdf

2. The world of plastics, in numbers. Accessed June 4, 2021. https://theconversation.com/the-world-of-plastics-in-numbers-100291

3. Soares JBP, McKenna TFL. *Polyolefin Reaction Engineering*. Wiley-VCH Verlag GmbH & Co. KGaA; 2012. doi:10.1002/9783527646944

4. Popli R, Mandelkern L. Influence of structural and morphological factors on the mechanical properties of the polyethylenes. *J Polym Sci Part B Polym Phys*. 1987;25(3):441-483. doi:10.1002/polb.1987.090250301

5. Soares JBP. Polyolefins with Long Chain Branches Made with Single-Site Coordination Catalysts: A Review of Mathematical Modeling Techniques for Polymer Microstructure. *Macromol Mater Eng*. 2004;289(1):70-87. doi:10.1002/mame.200300350

6. Demirors M. The history of polyethylene. In: *ACS Symposium Series*. Vol 1080. American Chemical Society; 2011:115-145. doi:10.1021/bk-2011-1080.ch009

7. Chadwick JC, Garoff T, Severn JR. Traditional Heterogeneous Catalysts. In: *Tailor-Made Polymers: Via Immobilization of Alpha-Olefin Polymerization Catalysts*. John Wiley and Sons; 2008:43-78. doi:10.1002/9783527621668.ch2

8. Srinivasa Reddy S, Radhakrishnan K, Sivaram S. Methylaluminoxane: Synthesis, characterization and catalysis of ethylene polymerization. *Polym Bull*. 1996;36(2):165-171. doi:10.1007/bf00294902

9. Hamielec AE, Soares JBP. Polymerization reaction engineering - Metallocene catalysts. *Prog Polym Sci*. 1996;21(4):651-706. doi:10.1016/0079-6700(96)00001-9

10. Kissin Y V. Multicenter nature of titanium-based Ziegler-Natta catalysts: Comparison of ethylene and propylene polymerization reactions. *J Polym Sci Part A Polym Chem*. 2003;41(12):1745-1758. doi:10.1002/pola.10714

11. Kissin Y V. Main kinetic features of ethylene polymerization reactions with heterogeneous Ziegler-Natta catalysts in the light of a multicenter reaction mechanism. *J Polym Sci Part A Polym Chem*. 2001;39(10):1681-1695. doi:10.1002/pola.1146

12. Soares JBP. Mathematical modelling of the microstructure of polyolefins made by coordination polymerization: A review. *Chem Eng Sci*. 2001;56(13):4131-4153. doi:10.1016/S0009-2509(01)00083-5

13. Soares JBP, Hamielec AE. Deconvolution of chain-length distributions of linear polymers made by multiple-site-type catalysts. *Polymer (Guildf)*. 1995;36(11):2257-2263.

doi:10.1016/0032-3861(95)95305-K

14. Soares JBP, Hamielec AE. General dynamic mathematical modelling of heterogeneous Ziegler-Natta and metallocene catalyzed copolymerization with multiple site types and mass and heat transfer resistances. *Polym React Eng*. 1995;3(3).

15. Soares JBP, Hamielec AE. Bivariate chain length and long chain branching distribution for copolymerization of olefins and polyolefin chains containing terminal double-bonds. *Macromol Theory Simulations*. 1996;5(3):547-572. doi:10.1002/mats.1996.040050310

16. Nguyen TQ, Kausch HH. Molecular Weight Distribution — Characterisation by GPC. In: Springer, Dordrecht; 1999:151-155. doi:10.1007/978-94-015-9231-4_33

17. Nguyen TQ, Kausch HH. Molecular Weight Distribution and Mechanical Properties. In: Springer, Dordrecht; 1999:143-150. doi:10.1007/978-94-015-9231-4_32

18. Cambridge Polymer Group :: GPC/SEC. Accessed June 5, 2021. https://www.campoly.com/cpg-services/analytical-testing/chromatography/gpcsec/

19. Elements of Polymer Science & Engineering - 2nd Edition. Accessed June 5, 2021. https://www.elsevier.com/books/elements-of-polymer-science-and-engineering/rudin/978-0-12-601685-7

20. Al-Khazaal AZ, Soares JBP. Characterization of ethylene/α-olefin copolymers using high-temperature thermal gradient interaction chromatography. *Macromol Chem Phys*. 2014;215(5):465-475. doi:10.1002/macp.201300736

21. Grubisic Z, Rempp P, Benoit H. A universal calibration for gel permeation chromatography. *J Polym Sci Part B Polym Lett*. 1967;5(9):753-759. doi:10.1002/pol.1967.110050903

22. Roedel MJ. The Molecular Structure of Polyethylene. I. Chain Branching in Polyethylene during Polymerization. *J Am Chem Soc*. 1953;75(24):6110-6112. doi:10.1021/ja01120a005

23. João B. P. Soares, R. F. Abbott, J. D. Kim. Environmental stress cracking resistance of polyethylene: The use of CRYSTAF and SEC to establish structure–property relationships. Accessed June 5, 2021. https://onlinelibrary.wiley.com/action/showCitFormats?doi=10.1002%2F%28SICI%291099-0488%2820000515%2938%3A10%3C1267%3A%3AAID-POLB10%3E3.0.CO%3B2-5

24. Nishikida K, Housaki T, Morimoto M, Kinoshita T. Gel permeation chromatography-Fourier transform infrared study of some synthetic polymers. II. Instrumentation for the characterization of polyethylene. *J Chromatogr A*. 1990;517(C):209-217. doi:10.1016/S0021-9673(01)95722-X

25. Menczel JD, Prime RB. *Thermal Analysis of Polymers: Fundamentals and Applications*. John Wiley and Sons; 2008. doi:10.1002/9780470423837

26. Menczel JD, Judovits L, Prime RB, Bair HE, Reading M, Swier S. Differential Scanning Calorimetry (DSC). In: *Thermal Analysis of Polymers: Fundamentals and Applications*. John Wiley and Sons; 2008:7-239. doi:10.1002/9780470423837.ch2

27. Thermal Analysis of Polymers | Wiley Online Books. Accessed June 5, 2021. https://onlinelibrary.wiley.com/doi/book/10.1002/9780470423837

28. Cossoul E, Baverel L, Martigny E, Macko T, Boisson C, Boyron O. Homogeneous copolymers of ethylene with α-olefins synthesized with metallocene catalysts and their use as standards for TREF calibration. *Macromol Symp*. 2013;330(1):42-52. doi:10.1002/masy.201300022

29. Saadat S. Polymerization Kinetics of Ethylene/1-Hexene Copolymers Made with Two Metallocene Catalysts. Published online 2018. doi:10.7939/R3639KM27

30. Wild L, Ryle TR, Knobeloch DC, Peat IR. Determination of branching distributions in polyethylene and ethylene copolymers. *J Polym Sci Polym Phys Ed*. 1982;20(3):441-455. doi:10.1002/POL.1982.180200307

31. Monrabal B. Crystallization analysis fractionation: A new technique for the analysis of branching distribution in polyolefins. *J Appl Polym Sci*. 1994;52(4):491-499. doi:10.1002/app.1994.070520403

32. Monrabal B, Sancho-Tello J, Mayo N, Romero L. Crystallization elution fractionation. A new separation process for polyolefin resins. In: *Macromolecular Symposia*. Vol 257. John Wiley & Sons, Ltd; 2007:71-79. doi:10.1002/masy.200751106

33. Boor J. Ziegler-Natta Catalysts Polymerizations - 1st Edition. Accessed June 6, 2021. https://www.elsevier.com/books/ziegler-natta-catalysts-polymerizations/boor/978-0-12-115550-6

34. Natta G, Mazzanti G, Valvassori A, Sartori G, Fiumani D. Ethylene–propylene copolymerization in the presence of catalysts prepared from vanadium triacetylacetonate. *J Polym Sci*. 1961;51(156):411-427. doi:10.1002/pol.1961.1205115603

35. Dammert R, Heino E-L, Korvenoja T, Martinsson H-B. A Multimodal Polymer Composition. Published online June 29, 2000.

36. Monrabal B. Crystaf : Crystallization analysis fractionation. A new approach to the composition analysis of semicrystalline polymers. *Macromol Symp*. 1996;110(1):81-86. doi:10.1002/masy.19961100107

37. Monrabal B: Characterization of homogeneous ethylene/1-octene copolymers made with a single-site catalyst. CRYSTAF analysis and calibration - Monrabal - 1999 - Journal of Polymer Science Part A: Polymer Chemistry - Wiley Online Library. Accessed June 6, 2021. https://onlinelibrary.wiley.com/doi/abs/10.1002/%28SICI%291099-0518%2819990101%2937%3A1%3C89%3A%3AAID-POLA10%3E3.0.CO%3B2-%23

38. L. J. D. Britto, J.B.P. Soares. Polyolefin analysis by single-step crystallization fractionation - Britto - 1999 - Journal of Polymer Science Part B: Polymer Physics - Wiley

Online Library. Published online 1999. Accessed June 6, 2021. https://onlinelibrary.wiley.com/doi/abs/10.1002/%28SICI%291099-0488%2819990315%2937%3A6%3C539%3A%3AAID-POLB6%3E3.0.CO%3B2-O

39. Rudin A, Choi P. The Elements of Polymer Science and Engineering. *Elem Polym Sci Eng*. Published online 2013.

40. Pérez O, Soares JBP. Coordination Polymerization. In: *Handbook of Polymer Synthesis, Characterization, and Processing*. John Wiley and Sons; 2013:85-104. doi:10.1002/9781118480793.ch5

41. Anantawaraskul S, Bongsontia W, Soares JBP. Simultaneous deconvolution of molecular weight and chemical composition distribution of ethylene/1-olefin copolymers: Strategy validation and comparison. *Macromol React Eng*. 2011;5(11-12):549-562. doi:10.1002/mren.201100032

42. Alfonso A, Palacios C. *Polymerization Kinetics and Structure-Property Relationships of Ethylene/1-Hexene Copolymers*.; 2018. doi:10.7939/R30000G3K

43. Zurek E, Ziegler T. Theoretical studies of the structure and function of MAO (methylaluminoxane). *Prog Polym Sci*. 2004;29(2):107-148. doi:10.1016/j.progpolymsci.2003.10.003

44. Da Silva Filho AA, Soares JBP, De Galland GB. Measurement and mathematical modeling of molecular weight and chemical composition distributions of ethylene/α-olefin copolymers synthesized with a heterogeneous Ziegler-Natta catalyst. *Macromol Chem Phys*. 2000;201(12):1226-1234. doi:10.1002/1521-3935(20000801)201:12<1226::AID-MACP1226>3.0.CO;2-W

45. Soares JBP, Abbott RF, Willis JN, Liu X. A new methodology for studying multiple-site-type catalysts for the copolymerization of olefins. *Macromol Chem Phys*. 1996;197(10):3383-3396. doi:10.1002/macp.1996.021971025

46. Alfonso A, Palacios C. Anuar Alfonso Caldera Palacios. Published online 2018.

47. Kissin Y. Alkene Polymerization Reactions with Transition Metal Catalysts. *Stud Surf Sci Catal*. 2007;173:419-570. Accessed July 20, 2021. http://www.sciencedirect.com/science/article/pii/S0167299107000067

48. Soares JBP, Anantawaraskul S. Crystallization analysis fractionation. *J Polym Sci Part B Polym Phys*. 2005;43(13):1557-1570. doi:10.1002/polb.20441

Appendix A: Polymerization Synthesis Conditions of the ZN Polymer and its Microstructural Parameters

Sample ID	H_2 (PSI)	1-Hexene (g)	Ethylene (PSI)	Temperature (°C)	Catalyst (g)	TEA (g)
ZN Polymer	40	30	70	90	0.02	0.496

Sample ID	M_w	M_n	PDI	$\overline{SCB}$	$\bar{F}_B$	$\bar{T}$ (°C)
ZN Polymer	58,092	9,879	5.88	11.77	0.025	83.26

Appendix B: Polymerization Synthesis Conditions for Polymers Made Using Bis(cyclopentadienyl) hafnium (IV) dichloride and Their Microstructural Parameters

Sample ID	H_2 (PSI)	1-Hexene (g)	Ethylene (PSI)	Temperature (°C)	Catalyst (µmol)	MAO (g)
H1	31.82	6.86	165	120	0.3	6.45
H2	13.18	6.86	165	120	0.3	6.45
H3	22.5	10.50	165	120	0.3	6.45
H4	31.82	14.14	165	120	0.3	6.45
H5	22.5	10.50	165	120	0.3	6.45
H6	22.5	10.50	165	120	0.3	6.45
H7	13.18	14.14	165	120	0.3	6.45
H8	45	10.50	165	120	0.3	6.45
H9	22.5	10.50	165	120	0.3	6.45
H10	22.5	10.50	165	120	0.3	6.45
H11	22.5	1.00	165	120	0.3	6.45
H12	22.5	1.00	165	120	0.3	6.45
H13	0	10.50	165	120	0.3	6.45
H14	13.18	6.86	165	120	0.3	6.45

H15	22.5	1.00	165	120	0.3	6.45
H16	13.18	14.14	165	120	0.3	6.45
H17	0	10.50	165	120	0.3	6.45
H18	31.82	14.14	165	120	0.3	6.45
H19	31.82	6.86	165	120	0.3	6.45
H20	45	10.50	165	120	0.3	6.45
H21	22.5	1.00	165	120	0.3	6.45
H23	45	20.00	100	120	0.3	6.45
H26	0	10.50	200	120	0.3	6.45
H27	0	10.50	200	120	0.3	6.45
H28	6.5	10.00	165	120	0.3	6.45
H29	0	10.50	275	120	0.3	6.45
H31	0	7.84	180	120	0.3	6.45
H32	2.6	4.33	165	120	0.3	6.45
H33	2.6	4.33	165	120	0.3	6.45
H36	0	10.50	275	108	0.07	1.6125
H37	0	10.50	275	111	0.07	1.6125
H38	45	6.19	80	120	0.3	6.45
H39	45	6.19	100	120	0.3	6.45
H40	0	7.19	165	120	0.07	1.6125
H41	0	6.54	150	120	0.07	1.6125
H42	45	2.65	100	120	0.3	6.45
H43	45	4.25	100	120	0.3	6.45
H44	45	3.50	100	120	0.3	6.45
H45	45	2.10	60	120	0.3	6.45
H46	45	2.80	80	120	0.3	6.45
H47	45	3.40	80	120	0.3	6.45
H52	3.5	4.00	165	120	0.3	6.45
H53	3.5	4.00	165	120	0.3	6.45
H54	3	4.00	165	120	0.3	6.45
H55	5	4.00	165	120	0.3	6.45
H56	6.5	4.00	165	120	0.3	6.45
H57	8	4.00	165	120	0.3	6.45
H58	10	4.00	165	120	0.3	6.45
H59	13.18	11.52	165	120	0.3	6.45
H60	13.18	14.78	165	120	0.3	6.45
H61	13.18	13.15	165	120	0.3	6.45
H63	13.18	9.89	165	120	0.3	6.45
H65	13.18	8.26	165	120	0.3	6.45
H66	0	5.95	165	120	0.07	1.6125

H69	0	4.80	150	120	0.07	1.6125
H70	0	4.61	165	120	0.07	1.6125
H72	0	5.41	150	120	0.07	1.6125
H73	0	4.19	150	120	0.07	1.6125
H74	0	4.32	135	120	0.07	1.6125
H75	0	4.87	135	120	0.07	1.6125
H76	0	3.77	135	120	0.07	1.6125
H77	0	3.00	135	120	0.07	1.6125
H78	0	2.00	135	120	0.07	1.6125
H79	0	1.00	135	120	0.07	1.6125
H80	0	8.00	275	105	0.07	1.6125
H82	0	4.00	275	105	0.07	1.6125
H83	0	2.00	275	105	0.07	1.6125
H84	0	1.00	275	105	0.07	1.6125

Sample ID	**M_w**	**M_n**	**PDI**	**$\overline{SCB}$**	**$\bar{F}_B$**	**$\bar{T}$ (°C)**
H1	7,395	3,645	2.03	21.21	0.046	71.80
H2	16,003	7,787	2.06	6.88	0.014	91.51
H3	5,385	2,686	2.00	16.23	0.035	78.57
H4	6,621	3,318	2.00	14.40	0.031	80.99
H5	7,776	3,878	2.01	11.78	0.025	84.39
H6	6,961	3,449	2.02	15.11	0.032	80.06
H7	9,626	4,814	2.00	13.70	0.029	81.91
H8	5,196	2,599	2.00	14.84	0.032	80.41
H9	7,422	3,680	2.02	12.36	0.026	83.65
H10	7,175	3,536	2.03	12.08	0.025	84.00
H11	8,627	4,178	2.06	6.99	0.014	90.42
H12	8,890	4,413	2.01	6.89	0.014	90.54
H13	61,040	29,776	2.05	14.89	0.032	80.35
H14	10,643	5,013	2.12	14.17	0.030	83.83
H15	8,623	4,164	2.07	7.06	0.015	90.32
H16	8,923	4,495	1.99	23.54	0.052	67.96
H17	62,618	30,802	2.03	14.38	0.031	81.01
H18	6,281	3,310	1.90	23.25	0.051	68.94
H19	5,931	3,127	1.90	17.67	0.038	76.65
H20	4,949	2,811	1.76	21.21	0.046	68.40

H21	7,457	3,660	2.04	8.10	0.017	89.04
H23	3,383	2,120	1.60	46.10	0.113	32.98
H26	110,524	49,841	2.22	11.43	0.024	84.84
H27	115,734	36,783	3.15	10.26	0.021	85.18
H28	15,900	7,700	2.06	14.50	0.031	82.78
H29	123,300	34,300	3.59	6.20	0.013	91.38
H31	114,071	52,009	2.19	7.66	0.016	89.59
H32	43,995	22,049	2.00	4.91	0.010	92.96
H33	40,758	20,150	2.02	5.54	0.011	90.54
H36	167,330	54,699	3.06	5.37	0.011	90.72
H37	152,575	55,072	2.77	5.31	0.011	89.94
H38	4,199	1,467	2.86	33.14	0.076	51.34
H39	3,189	1,814	1.76	26.17	0.058	51.22
H40	70,229	33,863	2.07	7.63	0.016	87.16
H41	84,197	40,997	2.05	7.70	0.016	86.55
H42	3,947	2,068	1.91	18.27	0.039	84.55
H43	3,300	1,662	1.99	24.26	0.054	58.12
H44	3,455	1,838	1.88	22.16	0.049	71.88
H45	2,218	1,147	1.93	30.08	0.068	60.68
H46	3,362	2,207	1.52	19.23	0.042	74.81
H47	3,250	2,171	1.50	21.15	0.046	72.82
H52	35,951	16,251	2.21	5.31	0.011	90.12
H53	40,329	19,139	2.11	4.71	0.010	90.53
H54	42,138	19,643	2.15	4.30	0.009	90.92
H55	29,188	13,416	2.18	5.54	0.011	89.97
H56	29,575	12,850	2.30	5.17	0.011	90.32
H57	15,645	7,275	2.15	5.95	0.012	89.87
H58	15,866	7,280	2.18	6.56	0.013	89.69
H59	10,452	4,478	2.33	15.04	0.032	79.82
H60	13,071	6,287	2.08	12.11	0.025	82.99
H61	9,551	4,324	2.21	20.11	0.044	70.59
H63	10,777	4,806	2.24	13.72	0.029	81.56
H65	11,840	5,426	2.18	12.96	0.027	83.14
H66	103,517	44,010	2.35	6.62	0.014	87.65
H69	99,130	42,736	2.32	5.56	0.011	89.03
H70	112,606	48,659	2.31	4.49	0.009	90.12
H72	88,424	36,066	2.45	6.94	0.014	87.49
H73	90,800	30,500	2.98	5.60	0.011	87.93
H74	83,000	39,100	2.12	7.50	0.015	86.19
H75	84,100	31,800	2.65	7.00	0.014	86.33

H76	97,100	36,900	2.63	5.20	0.011	89.16
H77	100303	40941	2.45	1.00	0.002	95.21
H78	112,005	47,448	2.36	2.34	0.005	92.48
H79	103,021	48,577	2.12	1.48	0.003	94.94
H80	254,299	108,461	2.34	3.16	0.006	90.51
H82	259,849	105,249	2.47	1.20	0.002	93.46
H83	321,264	150,523	2.13	1.20	0.002	96.20
H84	345,555	159915	2.16	0.43	0.001	97.63

Appendix C: Polymerization Synthesis Conditions for Polymers Made Using CGC-Ti and Their Microstructural Parameters

Sample ID	H2 (PSI)	1-Hexene (g)	Ethylene (PSI)	Temperature (°C)	Catalyst (µmol)	MAO (g)
CGC5	5	7	110	120	0.132	2
CGC6	10	7	110	120	0.132	2
CGC7	20	7	110	120	0.132	2
CGC8	0	6	110	60	0.132	2
CGC9	0	3.5	110	80	0.132	2
CGC10	0	1.3	110	100	0.132	2
CGC11	35	19	110	120	0.132	2
CGC12	45	18	140	120	0.132	2
CGC13	0	4	180	120	0.132	2
CGC15	0	4	250	120	0.132	2
CGC16	0	9.8	56	120	0.180	2.72
CGC18	0	21.5	165	120	0.132	2
CGC19	35	21.5	172	120	0.265	4
CGC20	10	6.5	120	120	0.132	2
CGC21	0	6.5	120	120	0.132	2
CGC22	14.5	7.6	120	120	0.132	2
CGC23	5	6.1	120	120	0.132	2
CGC24	1.6	3.8	120	120	0.132	2
CGC25	5	4.7	120	120	0.132	2
CGC26	1.6	2.4	120	120	0.132	2
CGC30	2	1.9	120	120	0.132	2
CGC31	2	1.8	120	120	0.132	2
CGC32	0	1.8	120	120	0.066	1
CGC33	0	2.2	190	120	0.132	2

CGC34	0	2.25	195	120	0.132	2
CGC36	27	3	120	120	0.530	8
CGC37	32	1.15	50	120	0.530	8
CGC38	0	1.2	50	120	0.530	8
CGC39	0	2.45	210	120	0.132	2
CGC40	3	2	120	120	0.066	1
CGC41	4	2	120	120	0.066	1
CGC42	0	1.7	110	120	0.066	1
CGC43	2	1.9	120	120	0.132	2
CGC44	0	2.25	195	120	0.132	2
CGC45	32	1.15	50	120	0.530	8
CGC46	0	1.2	50	120	0.530	8
CGC47	0	1.7	110	120	0.066	1
CGC48	3	2	120	120	0.066	1
CGC49	0	2.25	195	120	0.044	0.66
CGC50	50	0.8	50	120	0.530	8
CGC51	40	0.8	50	120	0.530	8
CGC52	32	1.15	50	120	0.530	8
CGC53	0	1.2	50	120	0.530	8

Sample ID	**M_w**	**$\overline{SCB}$**	**$\bar{F}_B$**
CGC5	26,700	45.7	0.112
CGC6	28,600	42.2	0.102
CGC7	24,800	39.9	0.095
CGC8	400,000	56.3	0.145
CGC9	259,000	46.5	0.114
CGC10	224,600	15.5	0.033
CGC11	7,800	95.5	0.309
CGC12	7,300	82.8	0.248
CGC13	175,100	23.3	0.051
CGC15	261,400	13.2	0.028
CGC16	13,600	118.7	0.452
CGC18	82,000	72.2	0.203
CGC19	35,600	70.8	0.198
CGC20	37,400	34.3	0.080
CGC21	87,500	40.6	0.097
CGC22	25,800	40.9	0.098
CGC23	26,500	45	0.110
CGC24	35,700	29.6	0.067
CGC25	34,300	26	0.058

CGC26	43,800	14.7	0.031
CGC30	36,600	10.4	0.022
CGC31	58,400	8.5	0.018
CGC32	276,000	11.7	0.025
CGC33	476,400	7.4	0.015
CGC34	239,200	13.5	0.029
CGC36	228,100	12.1	0.025
CGC37	14,300	33	0.076
CGC38	36,000	27.5	0.062
CGC39	327,800	12.2	0.026
CGC40	41,000	12.6	0.027
CGC41	21,800	12.3	0.026
CGC42	82,400	18.1	0.039
CGC43	34,507	9.1	0.019
CGC44	200,440	13.3	0.028
CGC45	34,676	33.8	0.078
CGC46	24,217	26.6	0.060
CGC47	204,574	11.9	0.025
CGC48	25,088	12.6	0.027
CGC49	487,683	7.6	0.016
CGC50	16,619	32.2	0.074
CGC51	4,579	39.7	0.094
CGC52	4,376	54.7	0.140
CGC53	39,487	18.6	0.040